

Ain Sume

Recognition of Ground Targets with Polarimetric Seeker Radar at 94 GHz

SWEDISH DEFENCE RESEARCH AGENCY

Sensor Technology
P.O. Box 1165
SE-581 11 Linköping

FOI-R--0180--SE

September 2001

ISSN 1650-1942

Scientific report

Ain Sume

Recognition of Ground Targets with Polarimetric Seeker Radar at 94 GHz

| | | |
|---|---|---|
| Issuing organization FOI – Swedish Defence Research Agency Sensor Technology P.O. Box 1165 SE-581 11 Linköping | Report number, ISRN FOI-R--0180--SE | Report type Scientific report |
| | Research area code 5. Combat | |
| | Month year September 2001 | Project no. E3003 |
| | Customers code 5. Contracted Research | |
| | Sub area code 51 Weapons and Protection | |
| Author/s (editor/s) Ain Sume | Project manager Leif Carlsson | |
| | Approved by Johan Söderström | |
| | Scientifically and technically responsible Ain Sume | |
| Report title Recognition of Ground Targets with Polarimetric Seeker Radar at 94 GHz | | |
| Abstract (not more than 200 words) <p>The report investigates the use of radar polarimetry for improving ground target recognition with a mm-wave seeker radar at 94 GHz. Modelling and simulation are used for the investigation, in addition to an experiment of demonstrative character. The scenario is basically static, <i>i.e.</i> no flight simulation is made. Four different box-shaped targets have been generated, on whose contours trihedral and dihedral-type reflectors are distributed to serve as scattering centres. The clutter is modelled on the same principle on a flat surface. Performance statistics have been generated by random draw of the missile azimuth position, keeping elevation and distance constant. Polarimetric features of the radar return are compared with corresponding data in a database of the four targets. The best match gives an estimate of target type and the azimuth angle. The range resolution and the angular density of catalogue data are taken as variable parameters, as is the polarimetric capability of the seeker: two types have been compared, <i>viz.</i> one fully polarimetric, and one operating with horizontal polarization only. Significantly better performance is obtained for the fully polarimetric sensor, which in addition requires high range resolution combined with a small angular increment in catalogue data for acceptable probabilities of correct classification. Ground clutter deteriorates performance severely. The experimental part of the work aims to show that a real system is capable of fulfilling a minimum requirement, <i>viz.</i> to recognize single reflectors of the types used as building blocks in the modelling. To this end, a coherent, fully polarimetric 94 GHz radar has been used to measure the backscatter from 23 single reflectors, treated as unknown objects. A careful polarimetric calibration procedure enabled error-free classification, and raised the possibility of determining the roll-angle of the dihedral-type reflectors with good accuracy.</p> | | |
| Keywords radar, polarization, seeker, millimetre waves, ground targets, clutter, modelling, simulation, classification | | |
| Further bibliographic information | Language Swedish | |
| | | |
| ISSN 1650-1942 | Pages 58 p. | |
| Price acc. to pricelist Security classification | | |

| | | |
|--|--|---|
| Utgivare Totalförsvarets Forskningsinstitut - FOI Sensorteknik Box 1165 581 11 Linköping | Rapportnummer, ISRN FOI-R--0180--SE | Klassificering Vetenskaplig rapport |
| | Forskningsområde 5. Bekämpning | |
| | Månad, år September 2001 | Projektnummer E3003 |
| | Verksamhetsgren 5. Uppdragsfinansierad verksamhet | |
| | Delområde 51 VVS med styrda vapen | |
| Författare/redaktör Ain Sume | Projektledare Leif Carlsson | |
| | Godkänd av Johan Söderström | |
| | Tekniskt och/eller vetenskapligt ansvarig Ain Sume | |
| Rapportens titel (i översättning) Igenkänning av markmål med polarimetrisk 94 GHz målsökarradar | | |
| Sammanfattning (högst 200 ord) <p>Rapporten belyser användningen av radarpolarimetri för förbättring av måligenkänning med en mm-vågsradar vid 94 GHz. Prestanda bestäms genom modellering och simulering; dessutom innehåller arbetet en experimentell del av demonstrationskaraktär. Simuleringarna gäller för i princip statisk geometri, dvs ingen bansimulering görs. Fyra olika lådformade mål har genererats, där reflektorer av trieder- och diedertyp fördelas över sidoytorna och utgör spridningscentra. Klotterbakgrunden skapas på ett plan enligt samma princip. Statistik för prestandabestämning har genererats genom att slumpa robotens vinkelposition i azimutled, med konstant elevation och avstånd från målet. Polarimetriska särdrag hos radarreturen jämförs med motsvarande data i en databas över de fyra målen. Bäst överensstämmelse ger ett estimat av måltyp och azimutvinkel. Avståndsupplösningen och vinkelsteget i katalogdata har tagits som varierbara parametrar, likaså målsökarutförandet beträffande polarisationen: två typer har jämförts, en fullpolarimetrisk (koherent), och en för horisontell polarisation enbart. Man får signifikant bättre prestanda för den fullpolarimetriska sensorn, vilket dessutom kräver hög avståndsupplösning kombinerad med hög vinkeltäthet hos katalogdata för att ge en acceptabel sannolikhet för korrekt klassificering. Markklotter försämrar prestanda kraftigt. Arbetets experimentella del syftar till att visa att ett verkligt system förmår uppfylla minimikravet att känna igen enstaka reflektorer av den typ som används för modelleringen. En koherent, polarimetrisk 94 GHz-radar har använts för att mäta upp den polarimetriska returen från 23 enskilda reflektorer, vilka behandlades som okända objekt. Med en noggrann polarimetrisk kalibrering erhöles felfri klassificering; dessutom kunde orienteringsvinkeln i roll-led bestämmas med god noggrannhet hos reflektorer av diedertyp.</p> | | |
| Nyckelord radar, polarisation, målsökare, millimetervågor, markmål, klotter, modellering, simulering, klassificering | | |
| Övriga bibliografiska uppgifter | Språk Svenska | |
| ISSN 1650-1942 | Antal sidor: 58 s. | |
| Distribution enligt missiv | Pris: Enligt prislista Sekretess | |

Contents

| | | |
|----------|---|-----------|
| 1 | INTRODUCTION | 7 |
| 2 | TARGET RECOGNITION; BASIC CONCEPTS | 8 |
| 3 | MODELLING | 9 |
| 3.1 | MODELLING BY SCATTERING CENTRES..... | 9 |
| 3.2 | THE BASIC REFLECTOR TYPES | 9 |
| 3.2.1 | <i>Choice</i> | 9 |
| 3.2.2 | <i>Theoretical basis</i> | 10 |
| 3.2.3 | <i>Discussion: stochastic and deterministic modelling</i> | 11 |
| 3.3 | TARGETS | 11 |
| 3.3.1 | <i>Type</i> | 11 |
| 3.3.2 | <i>Contour</i> | 12 |
| 3.3.3 | <i>Reflector distribution</i> | 12 |
| 3.3.3.1 | <i>Stochastic reflector generation.....</i> | 12 |
| 3.3.3.2 | <i>Deterministic reflector generation</i> | 13 |
| 3.3.4 | <i>Detailed generation of four targets.....</i> | 13 |
| 3.3.4.1 | <i>Target 1 (primary target, "tank")</i> | 13 |
| 3.3.4.2 | <i>Target 2 ("van-type truck with covered platform")</i> | 13 |
| 3.3.4.3 | <i>Target 3 ("truck with open platform")</i> | 14 |
| 3.3.4.4 | <i>Target 4 (random)</i> | 16 |
| 3.4 | GROUND CLUTTER | 16 |
| 4 | SIMULATION | 20 |
| 4.1 | OVERVIEW | 20 |
| 4.2 | SYSTEM PARAMETERS | 20 |
| 4.3 | CALCULATION OF THE TARGET ECHO | 21 |
| 4.4 | RECOGNITION PRINCIPLES | 22 |
| 4.4.1 | <i>Features</i> | 22 |
| 4.4.1.1 | <i>Sensor with single channel</i> | 23 |
| 4.4.1.2 | <i>Fully polarimetric coherent sensor</i> | 23 |
| 4.4.2 | <i>Comparison with reference catalogue profiles</i> | 24 |
| 4.5 | COMPUTER PROGRAM | 25 |
| 4.6 | CLASSIFICATION PERFORMANCE WITHOUT GROUND CLUTTER | 25 |
| 4.6.1 | <i>Variation of angle increment in catalogue data ($\Delta R=0.3$ m)</i> | 26 |
| 4.6.1.1 | <i>Angle increment 0.01°</i> | 26 |
| 4.6.1.2 | <i>Angle increment 0.1°</i> | 27 |
| 4.6.1.3 | <i>Angle increment 1.0°</i> | 27 |
| 4.6.1.4 | <i>Angle increment 2.0°</i> | 28 |
| 4.6.1.5 | <i>Angle increment 10°</i> | 29 |
| 4.6.2 | <i>Variation of range resolution ($\Delta Az=0.1^\circ$)</i> | 29 |
| 4.6.2.1 | <i>Range resolution 0.3 m</i> | 29 |
| 4.6.2.2 | <i>Range resolution 0.5 m</i> | 30 |
| 4.6.2.3 | <i>Range resolution 1.0 m</i> | 31 |
| 4.6.2.4 | <i>Range resolution 3.0 m</i> | 31 |
| 4.6.3 | <i>Probabilities of correct classification</i> | 32 |
| 4.6.4 | <i>Resolution and reflector separation</i> | 34 |
| 4.7 | PERFORMANCE WITH CLUTTER | 36 |
| 5 | EXPERIMENT | 37 |
| 5.1 | REFLECTOR MEASUREMENTS | 37 |
| 5.2 | POLARIMETRIC RECOGNITION | 39 |
| 6 | SUMMARY AND CONCLUSIONS | 42 |
| | APPENDIX POLARISATION CONCEPTS | 44 |
| A.1 | THE SCATTERING MATRIX | 44 |

| | | |
|------------|--|----|
| A.2 | TARGET DECOMPOSITION..... | 47 |
| A.3 | STOKES' POLARISATION DESCRIPTION, THE MUELLER MATRIX AND THE HUYNEN PARAMETERS | 48 |
| A.3.1 | <i>Stokes' parameters and the Mueller matrix</i> | 48 |
| A.3.2 | <i>Huynen's parameters</i> | 49 |
| A.4 | THE HUYNEN PARAMETERS FROM THE SCATTERING MATRIX..... | 51 |
| A.4.1 | <i>The computational problem</i> | 51 |
| A.4.2 | <i>The tilt angle ψ from diagonalization of the scattering matrix (Bickel, 1965)</i> | 52 |
| A.4.3 | <i>Special cases</i> | 55 |
| A.4.3.1 | <i>General dihedral</i> | 55 |
| A.4.3.2 | <i>Dihedral+helix</i> | 55 |
| A.4.3.3 | <i>Sphere+special dihedral</i> | 56 |
| REFERENCES | | 57 |

1 Introduction

This report is concerned with recognition of radar targets using the polarisation of electromagnetic waves. The application considered is the discrimination of ground targets by a polarimetric mm-wave radar at 94 GHz, operating in a missile seeker.

The missile is launched from a platform, *e.g.* a helicopter, and then acts autonomously (Figure 1.1). The radar teams with a passive IR sensor in a dual configuration, where the output data of the sensors are fused to enhance performance. For optimal use, it is essential that the function of each individual channel should be properly understood. This is the rationale behind the present work, where the radar is assumed to be the sole sensor.

One main objective of this study is to demonstrate the performance gain that a fully polarimetric radar provides over a single channel system working with one polarisation only. Another purpose is to quantify how the performance depends on range resolution. The radar is assumed to be of the real aperture type.

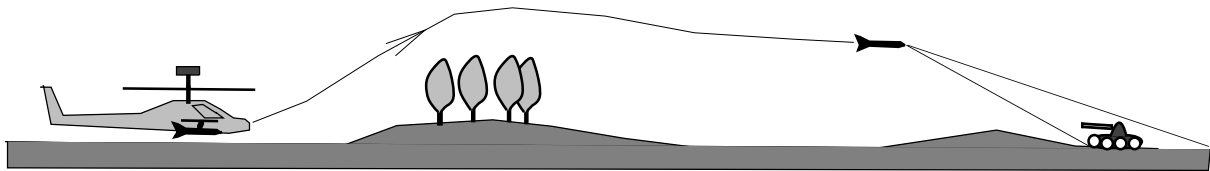


Figure 1.1 Possible scenario, with launch platform at left, and an autonomous missile at right, with a mm-radar seeker engaging a ground target.

The primary targets of interest are tanks. The main question is how well the radar can distinguish these from some other ground target types, drawing on polarimetric information to various extent. The work resorts to simulations in quantifying the discriminating capability of the sensor, using specially developed models for target and background. The novel feature here is the use of simple deterministic modelling throughout, both for the targets and the ground clutter. As an approximation, the backscatter is assumed to originate from scattering centres, consisting of reflectors of simple types with well-known polarisation transformation, distributed over the surfaces of the illuminated objects. This gives a reasonably accurate representation of the targets and the background (grass), while running times of the simulations are kept within manageable limits. Hence, variation of important parameters can be made (*e.g.* range resolution), to have direction for optimal choices.

The estimate of the most probable target candidate for a detected object is based upon a comparison of features in the radar return with corresponding quantities in a database of target exemplars. One significant question addressed is the required density of data in the database to ascertain an acceptable performance level.

Ultimately, findings of simulation must be put on a firm footing by experimentation. To this end, a simple experiment has been devised to demonstrate that a mm-wave radar possesses the ability to recognize the building blocks of the modelling, *i.e.* single reflectors of simple kind. If this ability turns out to be unattainable in practice, one can hardly hope to succeed in the overall task of recognizing a whole target. For this demonstration, a coherent, fully polarimetric 94 GHz radar has been used, in a ground-based static set-up.

The work is a part of the activities in the IRmm Multisensor project, currently running at the FOI (previously FOA).

2 Target recognition; basic concepts

Target recognition¹ consists in many cases of the reception of a signal from a target and a comparison with internal representations of various **objects**, followed by a decision whether there is a correspondence or not. As a rule, the received signal is not used directly for the comparison; the search for a limited number of **features** (or attributes), with which a conception of an object may be built up, is a key step in the recognition, which thus may be regarded as a process of recognizing common features (Bar-Yam, 1997, p. 395), see Figure 2.1.

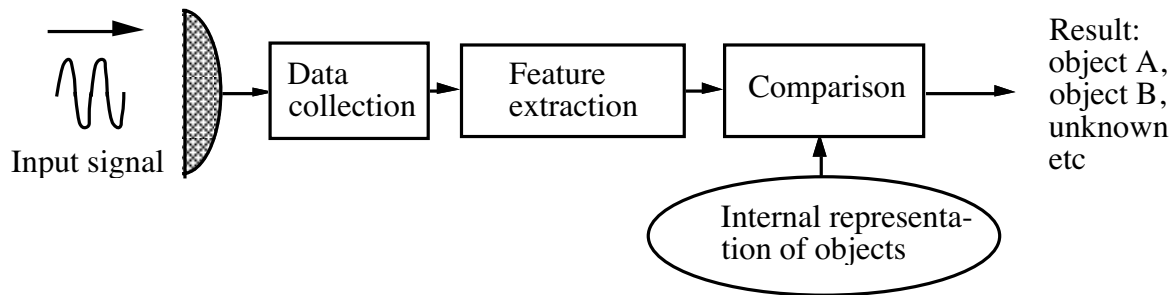


Figure 2.1 Schematic description of target recognition.

The features are sensor dependent. Examples of feature categories in the case of human vision are colour, shape, and movement. With radar, potentially all quantities that characterize an electromagnetic wave are available for feature generation: amplitude, frequency (wavelength), phase, polarisation, and direction of propagation (Figure 2.2).

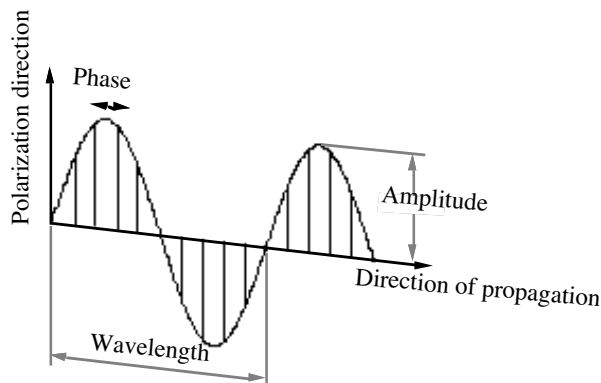


Figure 2.2 The instantaneous electric field of a sinusoidal electromagnetic wave. The wave is characterized by its amplitude, wavelength (frequency), phase, polarisation (=direction of the field vector) and direction of propagation.

A well chosen feature is robust, which means that it does not vary for moderate changes in the target/sensor arrangement. Again, taking human vision as an example, *shape* is a robust property of rigid objects. In the case of radar, one strategy is to model on this, and use radar parameters related to shape. The opposite strategy is to employ features with no direct correspondence in our natural, visual image formation, *e.g.* doppler shift. The present work represents the latter approach, using features related to the polarisation of the wave. Another characteristic is that the chosen features are *not* generally robust; they fluctuate rapidly when the aspect angle changes. The internal representation of the objects in Figure 2.1 will consist of a database of features of target candidates.

¹ For an overview of automatic target recognition see *e.g.* Dudgeon and Lacoss (1993).

3 Modelling

3.1 Modelling by scattering centres

The target modelling follows the principles laid down in previous FOA work (Kjellgren *et al.*, 1992, 1993). The basic assumption is that the monostatic scattering of a short-wavelength² radar wave can be approximated by the coherent sum of contributions from discrete scattering centres on the surfaces of the target, with specific polarisation transformation properties, expressed by a polarisation (or scattering) matrix³. The modelling in the mentioned references was based on imaging measurements of the kind shown in Figure 3.1, illustrating the occurrence of scattering centra. Some of these could be identified with simple geometrical structures on the tank.

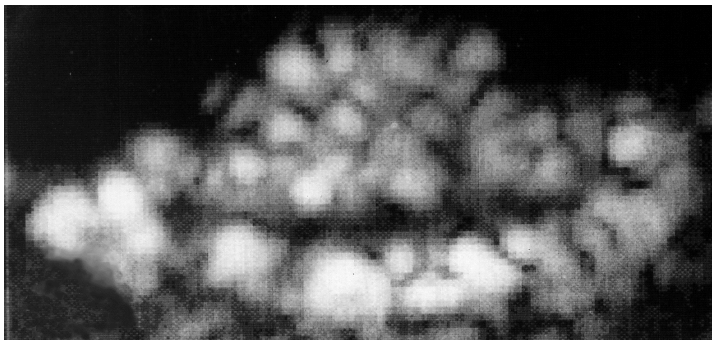


Figure 3.1 Radar image of a Centurion tank, seen 45° from the front aspect, 12° elevation. The image illustrates that the radar signature is dominated by the returns from a number of scattering centres. The frequency is 94 GHz.

A model, generated on these principles, has two properties of importance for the application in question, besides the primary one of being polarimetric. Firstly, calculations of the radar return with scattering matrices are comparatively *fast*, even with a large number of scatterers. This is an obvious advantage when performance statistics are calculated from a large number of simulations. Secondly, it is simple to vary relevant parameters in a systematic way, an essential advantage if one wants to *understand* what is important for the target classification.

3.2 The basic reflector types

3.2.1 Choice

The scattering from a general centre can be viewed as the superposition of scatterings from reflector primitives, *i.e.* reflectors of simple kind with well-known scattering properties, satisfying certain criteria (see the next section and Appendix). The choice of these reflectors is not unique; here we take reflectors of two basic types, *viz.* dihedral and trihedral, for the model build-up.

² Shorter than characteristic dimensions of the individual scatterers.

³ A survey of these and other theoretical concepts is given in the Appendix.

The dihedral is realized by a cylinder "hat" [Figure 3.2 (a)] with a smoothly varying radar cross section, given by a simple expression for all aspect angles over a hemisphere where the cylinder axis points towards zenith, see Table A.1 in the Appendix. This property distinguishes it from a dihedral with two plane, perpendicular surfaces (diplane), which gives retro-reflection only for perpendicular incidence towards the intersection between the surfaces. Even if diplanes are found in real targets, the usefulness of the reflector type *e.g.* for tracking is ephemeral. The aim to have a geometric correspondence between the model and the target has therefore had to yield to the computational economy of generating a retro-reflection of dihedral type, that is slowly varying over broad angular intervals, as one component of the backscatter.

The trihedral scattering is taken to occur in three triangular planes [Figure 3.2 (b)]; it is described by an equally simple formula, see Table A.1 in the Appendix.

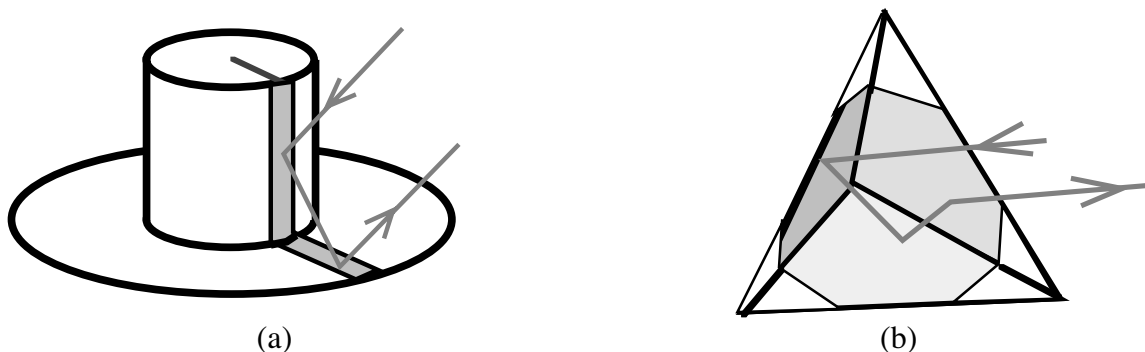


Figure 3.2 The two reflector types chosen for the build-up of the model by discrete scattering centres: (a) top-hat, and (b) trihedral corner reflector, with three perpendicular, triangular sides. Assuming that the wavelength is small compared to the reflector dimensions, the scattering can be analyzed in terms of rays, as in optics. The top-hat gives retro-reflection after two reflections ("even bounce"), the trihedral after three ("odd-bounce"). Only part of the respective reflector contributes to the radar return for a fixed aspect, as indicated by the shaded sections. The contributing part of the top-hat approximates to a plane dihedral.

3.2.2 Theoretical basis

The theoretical basis for the described procedure is that a general scattering matrix (symmetric) can be generated mathematically by a sum of three matrices, which correspond to reflectors of the two basic types (Kjellgren *et al.*, 1992), *viz.* one trihedral and two dihedrals. The latter ones form different tilt angles with the horizontal, with no interaction between them⁴. In the present case each scattering centre is not modelled as a general scatterer using three reflectors. Instead, only one reflector is used, either a top-hat or a corner, following a stochastic or a deterministic routine, as will be described in Section 3.3. If the real scatterer on a target has a clear-cut geometry, this may be a realistic representation, but often this will not be the case. However, in several target resolution cells and in all clutter resolution cells there will be a sufficient variety of reflectors in the model, to form the general kind of backscatter, so it is felt that the procedure is of sufficient generality. Verifying measurements will have to be made to substantiate this.

The two reflector types used for the modelling can be seen as members of two more general classes, "even bounce" and "odd-bounce", referring to the number of reflections a ray will experience, when its direction of propagation is reversed back towards the radar, if we use an optical view of the scattering.

⁴ This procedure is an application of the expansion of a general 2×2 matrix in some complete set, *e.g.* the Pauli matrices (see Appendix, section A.2).

The mentioned previous FOA work used the above principle for the modelling of a Centurion tank, at 94 GHz, as indicated in Figure 3.3.

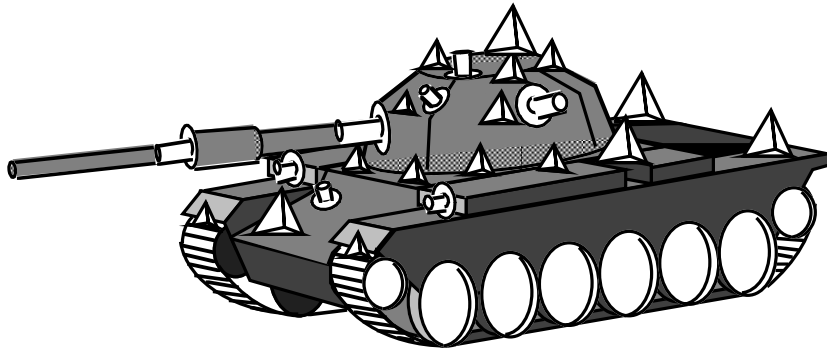


Figure 3.3 Modelling principle applied to a Centurion tank at 94 GHz (Kjellgren *et al.* 1992,1993). The radar backscatter is taken as the sum of the returns from discrete reflectors of dihedral or trihedral types (top-hats or bowls, and trihedrals, respectively); parts between the reflectors are neglected with respect to their radar properties.

The conditions for the optical approximation are not always fulfilled, especially in the case of ground clutter, which in the present work is represented by a large number of small reflectors. In this case the wavelength is not much smaller than characteristic reflector dimensions, and the simple optical view is no longer valid. The modelling principle should then be viewed as a mathematical postulation of scattering matrices of the two basic reflector types in points over the target contour, and a providing of a systematic calculation rule that describes how these matrices change with aspect angle. For the top-hats the rule is given by the right column in Table A.1 in the Appendix; for the trihedrals a $\cos^2 \delta$ -dependence is assumed, where δ is the angle between the symmetry axis of the reflector and the line-of-sight to the radar. This factor describes how the area of the effective reflector aperture [shaded in Figure 3.2 (b)], projected perpendicularly to the line of sight, changes with the radar position.

3.2.3 Discussion: stochastic and deterministic modelling

An alternative modelling would be to adopt some statistical distribution for the target and background returns, which is the procedure normally followed in studies of radar detection. Here, a deterministic modelling has been chosen deliberately to gain an impression of the usefulness of the method, even for the clutter. The model contains several variable parameters (reflector type, size, orientation, number), so it seems reasonable that real targets and clutter can be emulated with respect to *e.g.* the aspect dependence of the radar cross section, as well as spatial correlations and variations. With improving computer performance, relatively fast generation of realistic, coherent, polarimetric target and background signatures should be possible. One disadvantage of using the principle for the clutter is that the physical significance of the scattering centres begins to become lost, when reflector dimensions are less than the wavelength. A corresponding decrease of robustness of the model can be expected.

3.3 Targets

3.3.1 Type

Four different targets have been modelled along the lines described. One of them, a tank, is viewed as the primary candidate; the three other types have been generated to test the discriminating ability of the seeker. Two of these latter ones are intended to represent trucks

of somewhat different design, whereas the reflector composition of the third reflects no particular category; its generation proceeds mainly with random selection of parameters.

3.3.2 Contour

The four targets have been assumed to have the same shape and dimension. Each is approximated by a right-angled parallelepiped measuring $7.0 \times 3.6 \times 2.2$ m (length \times width \times height). The targets are oriented with their bottom surfaces horizontal; these surfaces rest on the ground. The reflectors are distributed over the other five sides.

The reason why not different target dimensions are assumed is that the work is focused on understanding the possibilities and limitations of *polarimetric* methods in the chosen application. Discriminating quantities have therefore been taken to be connected with wave polarisation as far as possible. Hence, target shape and dimension have not been given discriminating quality.

3.3.3 Reflector distribution

One target has been generated essentially by random draw of reflector parameters, while the other three have been given structure by deterministic assignment of the number of reflectors, their kind, sizes and orientations. Rectangular, non-overlapping sub-surfaces can be defined (Figure 3.4) on each target surface. The reflector generation within these sub-surfaces is made independently from the other sub-surfaces, choosing a deterministic or (partly) stochastic procedure.

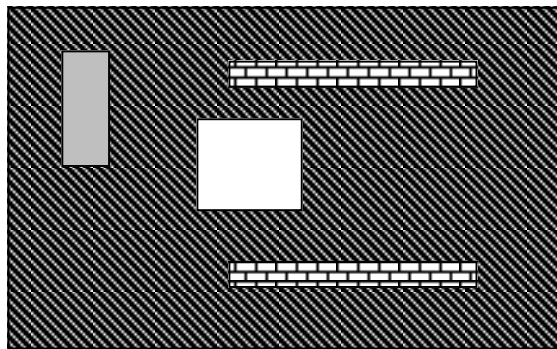


Figure 3.4 A rectangular surface on the box-shaped target can be divided into sub-rectangles, within which the reflector generation is made independently of the other sub-rectangles, and where a deterministic or a stochastic procedure for the generation can be chosen.

3.3.3.1 Stochastic reflector generation

If one chooses stochastic reflector generation within a sub-rectangle, the number ratio corners/hats, their respective number and summed radar cross section are chosen and fixed, whereas the position, orientation, and the individual **maximum radar cross section**⁵ of the reflectors are generated randomly. The latter quantity is drawn from a log-normal distribution with mean $m = -0.241629$ and standard deviation $s = 0.638025$. These values have been obtained from a log-normal fit to the distribution of the reflector sizes in the mentioned, previous FOA modelling of a Centurion tank. After the random assignment of the individual radar cross sections, their sum over the sub-surface is calculated. If the sum differs from the stipulated one, the individual cross sections are adjusted by a common factor to give zero difference.

⁵ *i.e.* the maximum radar cross section exhibited by the reflector, with optimal choice of polarisation and direction of illumination.

The radar cross section does not determine the top-hat dimensions uniquely. The quantity determined by the maximum radar cross section is rh^2 , alternatively $r(r' - r)^2$, depending on whether the effective retro-reflection area on the hat mantle is limited by the cylinder height h or by the radius r' of the circular plane, *cf.* Table A.1 in the Appendix. The quantity r is the radius of the cylinder. Only rh^2 , or alternatively $r(r' - r)^2$ enters the calculation of the field. For drawing the target figures, r has been arbitrarily set to 5 cm, whence h or r' can be calculated from the formulae in Table A.1.

The reflectors are distributed uniformly over the rectangle surface in question. In a corresponding fashion, they are assigned random orientations so that the symmetry axes of the trihedrals and hat cylinders are distributed uniformly over 2π solid angle, with the polar and azimuth angles drawn from uniform distributions over $[0, \pi/2]$ and $[0, 2\pi]$, respectively. The polar axis is normal to the target surface.

3.3.3.2 Deterministic reflector generation

In the deterministic procedure all the reflector parameters (type, size, number, position, orientation) are set manually within a rectangle.

3.3.4 Detailed generation of four targets

3.3.4.1 Target 1 (primary target, "tank")

For this target the mentioned previous FOA model of a Centurion tank has been used. All the reflectors in that model representing a scattering centre with a simple, clear-cut geometry, *i.e.* with scattering of pure dihedral or trihedral type, have been adopted with unchanged type, size and orientation. The position has been chosen with a subjective procedure, so that a Centurion-like target is retained. Seven wheels, modelled with bowls in the Centurion case, are now represented by top-hats, which have the same scattering matrix. The total number of these pure reflector types is 35, including the right side of the target, which was not modelled for Centurion; it is taken to be a mirror copy of the left side. The sum of the individual maximum cross sections⁶ equals 54 m². With high range resolution, the number of reflectors is considered too low; hence another 49 reflectors have been generated stochastically using the procedure described in section 3.3.3.1, with 50% of each basic type. These have been distributed in number in proportion to the size of the respective target surface, with 24 on the "roof", which is biggest. They have been placed on the hatched part of the surface in Figure 3.4, where no sub-rectangle has been defined. The summed maximum radar cross section of these reflectors is set to 25% of the corresponding sum for the deterministic reflectors on the whole rectangular side surface of the target, in accordance with the Centurion model.

A further four reflectors have been placed in the four upper corners of the object as points of reference for positioning of the range gates. The radar cross sections of these reflectors have been chosen so small as to be insignificant for the radar return. All four targets have been equipped with these markers.

After the completion of the reflector distribution, the target is fixed like a solid body. Figure 3.5 shows the generated target with the deterministically defined reflectors in red.

3.3.4.2 Target 2 ("van-type truck with covered platform")

This target has been constructed with a lab truck as a visual model, and with some guidance from radar data of similar objects. Reflectors have been postulated from a visual inspection of

⁶ As will be seen in section 4.4 the radar cross section is no strongly discriminating quantity in the clutter-free case, since the algorithm works with normalised quantities.

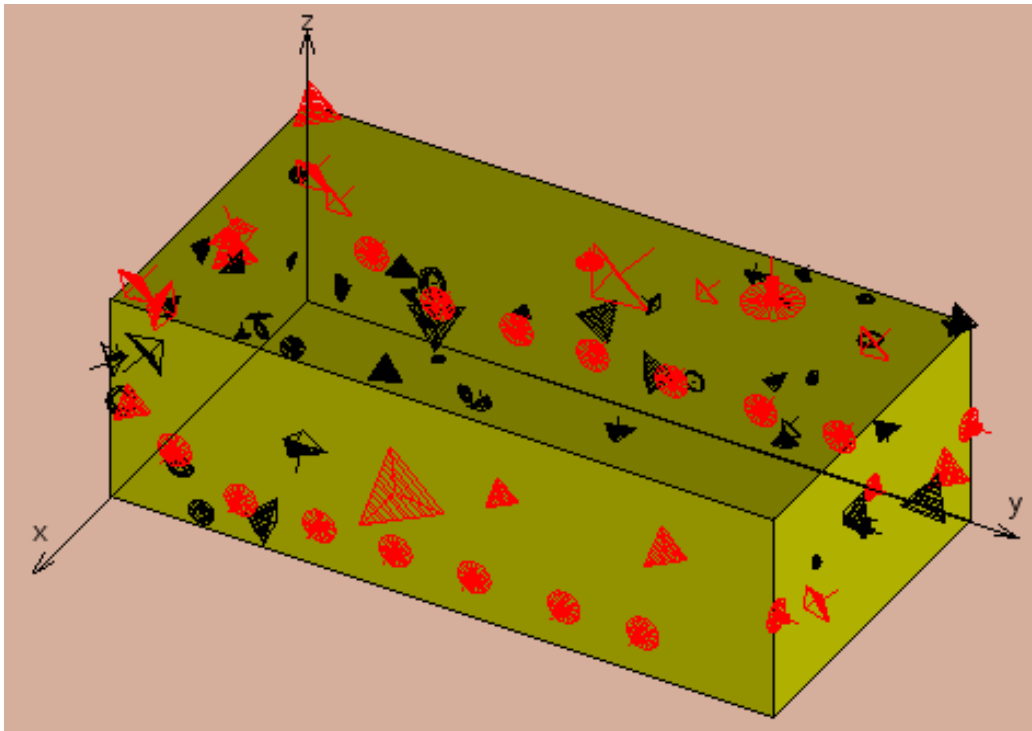


Figure 3.5 Radar model of the primary target type "tank", with deterministically defined reflectors (35) in red, representing ordered geometrical structures, *e.g.* the wheel rows on both sides. Reflectors generated stochastically (53) according to the procedure in the text are drawn in black. The trihedrals (with dashed apertures) have been magnified five times, in order to be seen in some detail, whereas the top-hats are in scale.

a FOI laboratory bus, with pure geometrical structures of hat and corner type (flanges, angle irons) given their corresponding counterparts in the model. The radar cross sections have been chosen from experience with the Centurion modelling and other target measurements at 94 GHz at the FOA, using ISAR (Inverse Synthetic Aperture Radar) technique. The type designation should hence be taken as a label of a somewhat fictive target. For the model to have better real-world footing, specific target radar cross section measurements are required.

The total number of deterministically defined reflectors is 31 whose summed maximum radar cross section is 22 m². Another 58 reflectors have been generated stochastically as for the previous target (the tank) to produce a target which can be used in studies with high spatial resolution. Their summed maximum radar cross section is 25% of that of the deterministic reflectors. The resulting model is shown in Figure 3.6.

3.3.4.3 Target 3 ("truck with open platform")

This model is intended to represent the same truck-like target as the previous one, but with no closed housing on the platform, which instead is assumed to be open, covering roughly the back half of the truck. It is assumed to be loaded with unstructured metal objects, represented by stochastically generated reflectors in the model, which in other respects is identical with Target 2. The total number of deterministically defined reflectors is 19, whose summed maximum radar cross section amounts to 15 m². Another 69 reflectors have been generated as for the previous target to produce a target which can be used in studies with high spatial resolution. Their summed maximum radar cross section is 25% of that of the deterministic reflectors for the respective target surface except for the "top" surface, which has been assumed to have the summed maximum cross section 25 m². The resulting model is shown in Figure 3.7.

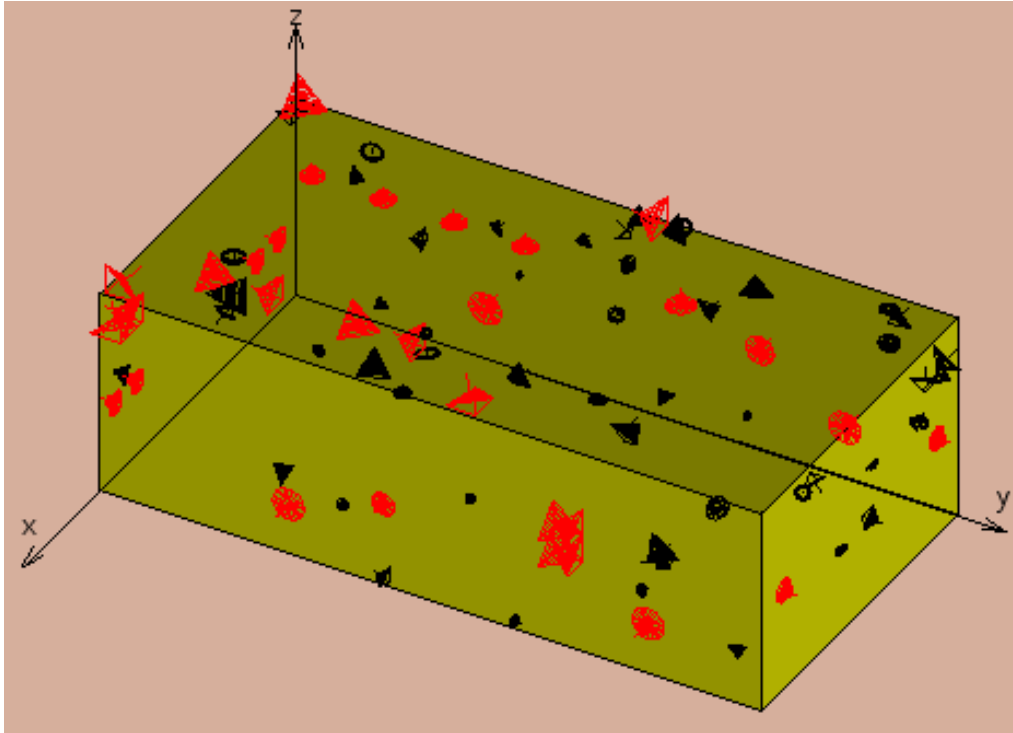


Figure 3.6 Radar target, modelled on a laboratory bus, essentially a truck with a closed housing on the platform. Deterministically defined reflectors (31) are drawn in red, representing ordered geometrical structures. Reflectors generated stochastically (58) according to the procedure in the text are drawn in black. The trihedrals (with dashed apertures) have been magnified five times, in order to be seen in some detail, whereas the top-hats are in scale.

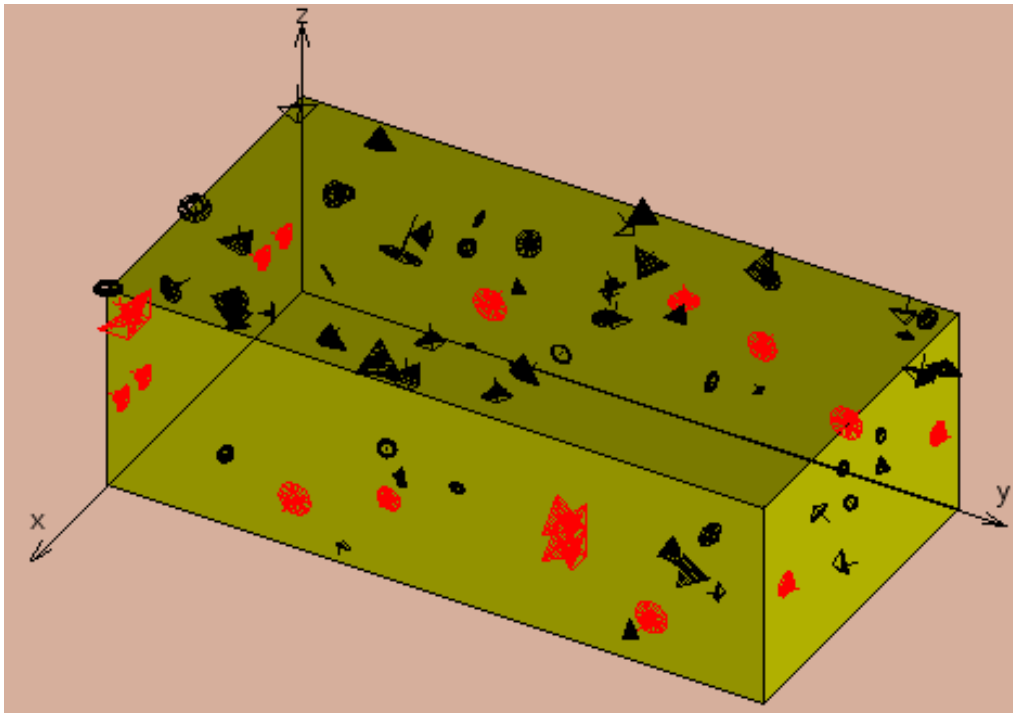


Figure 3.7 Radar model constructed on the same pattern as that in Figure 3.6, but with the covered platform replaced by an open one, loaded with unstructured metal objects, which are modelled with stochastically generated reflectors. In other respects the two models are identical. Deterministically defined reflectors (19) in red represent ordered geometric structures. Stochastically determined reflectors (69) are drawn in black. The trihedrals (with dashed apertures) have been magnified five times, in order to be seen in some detail, whereas the top-hats are in scale.

3.3.4.4 Target 4 (random)

The fourth target is of unspecified type. All its reflectors have been generated on the principles in section 3.3.3.1 with equal percentage of corners and top-hats. The total number of reflectors is 84, with 30 on the biggest surface (the "roof"), where the sum of the maximum radar cross sections of the reflectors is assumed to be 15 m². The number of reflectors on the other sides and their maximum radar cross section sum has been set proportional to the area of the respective target sides. Figure 3.8 depicts the model.

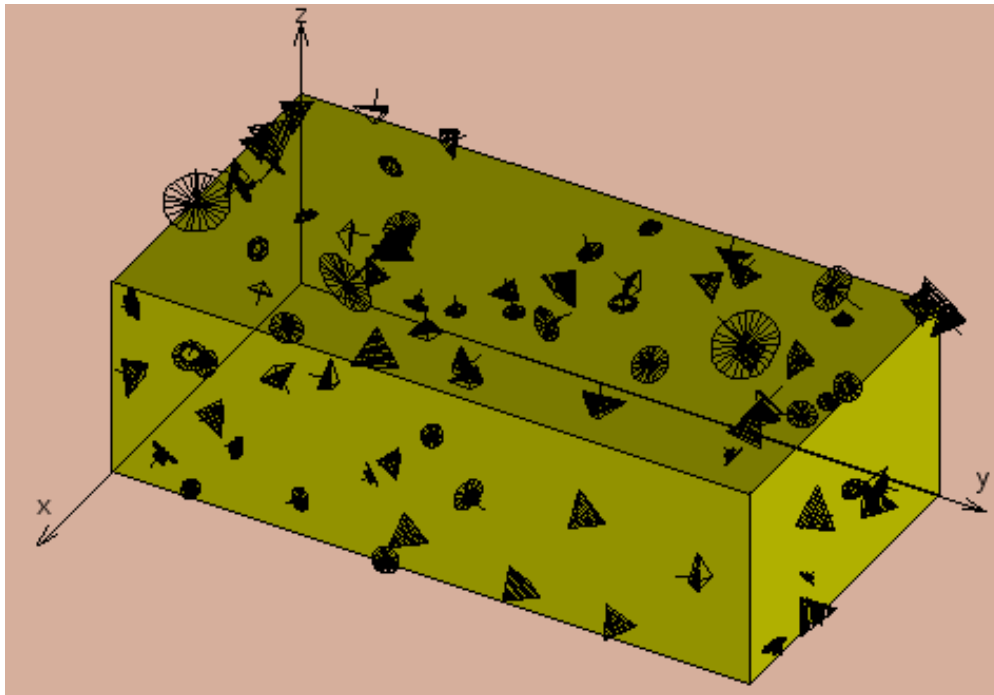


Figure 3.8 Model with all reflectors generated stochastically, with equal percentage (50%) corners and top-hats. The number of reflectors on the upper side has been set to 30; the sum of their maximum radar cross sections is 15 m². The other sides have the same surface density of reflectors, with the sum of maximum cross sections reduced in proportion to the size of the surface. The positions and orientations of the reflectors have been given random, uniform distributions. The trihedrals (with dashed apertures) have been magnified five times, in order to be seen in some detail, whereas the top-hats are in scale.

3.4 Ground clutter

For the clutter the same principle has been used as for the targets: it is modelled deterministically with top-hat and corner reflectors, distributed over a horizontal ground surface. The total number of reflectors and the percentage of the respective types are specified before the generation; then their sizes, positions and orientations are distributed randomly. Their number, size and orientation are parameters which determine the clutter mean and variance, which should agree with measured values at 94 GHz, determined under equal conditions. The most important of these are the incidence angle of the radar wave with respect to the ground surface (=the angle between the direction of propagation and the normal direction of the ground) and the spatial resolution.

For the clutter mean we calculate the value from the Georgia Institute of Technology (G.I.T.) ground clutter model at 94 GHz and 5° depression angle (Curry *et al.*, 1982,1987) which gives $\sigma^0 = 0.02465$ m²/ m² for grass. For the spatial variation we adopt, lacking better data, the value 5.7 dB for the log standard deviation of the clutter σ^0 , i.e.

$s_c = \sqrt{\text{VAR}(10^{10} \log \sigma^0)}$ [dB], measured with the M.I.T. Lincoln Laboratory 35 GHz airborne

SAR with 0.3 m spatial resolution (Novak and Netishen, 1992). We also adopt the same group's measured value 0.19 of the cross-polarised to like-polarised grass clutter reflectivity $E(|HV|^2)/E(|HH|^2)$, where E denotes mean value.

For the clutter model, the reflectors are spread uniformly over a square on the ground, whose side is chosen equal to the antenna footprint in the cross-range dimension measured between the 3 dB beamwidth points, 3 km from the radar. The number of reflectors can be chosen up to about 600000 [with present hardware]. The relative number of top-hats is set between 0 and 100%. Figure 3.9 shows an example of a target in ground clutter.

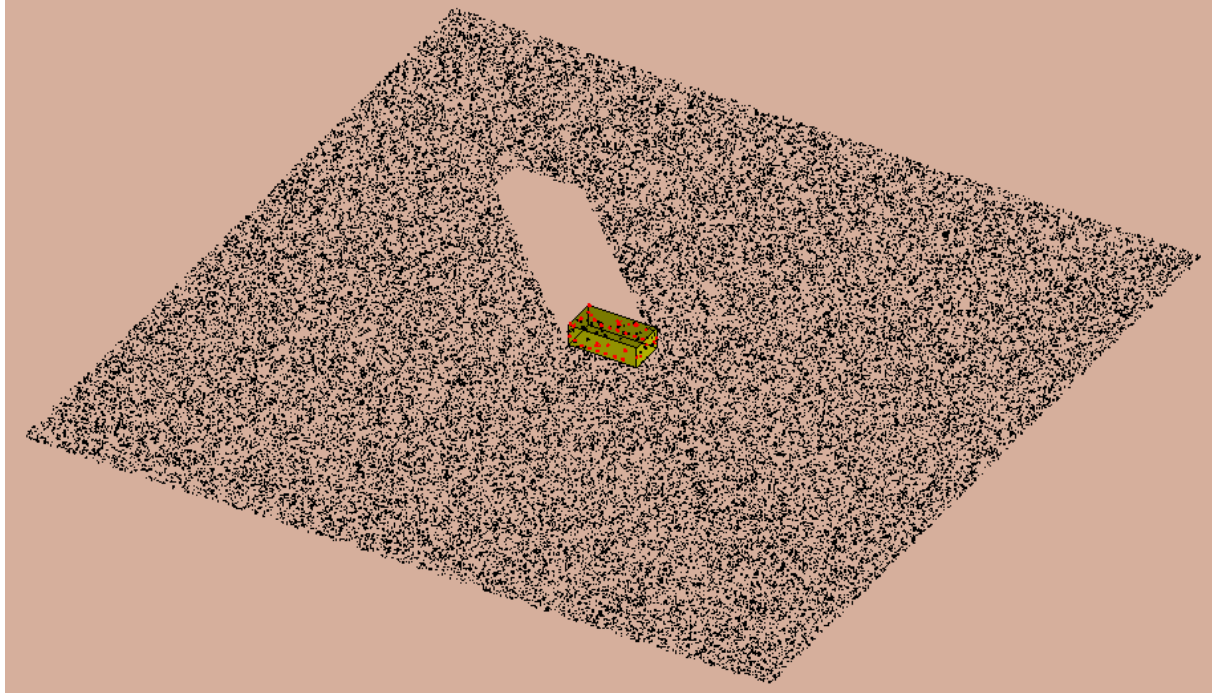


Figure 3.9 Example of modelling of ground clutter with 50000 reflectors, with 86% triangular corners and 14% top-hats. The clutter region is a square whose side is equal to the ground footprint of the 3 dB lobe width in cross-range of the antenna (diameter 0.15 m). The radar is at 3 km distance. The radar shadow appears on the ground; the missile seeker is at azimuth 45° from the forward direction of the target, and at 5° elevation.

The clutter model under study here allows variation of parameters, to have agreement between the simulated and the measured reflectivity values given in the last paragraph. The mean can be adjusted by proper choice of the number of reflectors and their dimensions. The maximum radar cross sections of the individual reflectors have been drawn from a log-normal distribution, with the mean $m = -0.241629$ and the standard deviation $s = 0.638025$, as for the targets. After the initial generation, the program monitors the clutter statistics in a simulated measurement of the reflectivity with a (SAR) sensor with 0.3 m × 0.3 m ground resolution. The maximum cross sections of the reflectors are then changed by a factor such that the mean reflectivity agrees with the G.I.T. model value. The resulting reflector configuration is then fixed and used for deterministic calculation of a coherently summed backscattered field for any azimuth location of the radar, in the same way as for the targets.

The spread (at 5° elevation) can be adjusted by varying the number of reflectors. Since this parameter had an upper limitation of about 600000 given the available computing power, another possibility was used to regulate the clutter standard deviation. It can be adjusted by limiting the polar angle interval $\Delta\theta$ over which the reflector symmetry axes are uniformly distributed. Nominally this angle is $\pi/2$ (horizontal to vertical orientation). By narrowing this value, the cross section spread due to varying orientation, is reduced.

The cross-polarised to co-polarised return ratio is dependent on the setting of the parameter which defines the number ratio between the top-hats and the trihedral corners. The following Table 3.1 lists parameter choices which gave agreement between the model and the mentioned measurements.

Table 3.1 Parameters in clutter model.

| Quantity | Value |
|---|---|
| Number of reflectors | 550000 |
| Percentage odd-type reflectors (trihedrals) | 86 % |
| Distribution of individual reflector maximum cross sections | log-normal with $m=-0.241629$, $s=0.638025$ |
| Distribution of top-hat symmetry axis | |
| polar angle | Uniform 35-60° |
| azimuth | Uniform 0-360° |
| Distribution of trihedral symmetry axis | |
| polar angle | Uniform 0-90° |
| azimuth | Uniform 0-360° |

Figure 3.10 shows histograms of the reflectivity σ^0 obtained from a simulated measurement with $0.3 \text{ m} \times 0.3 \text{ m}$ ground resolution in stochastically chosen directions within the clutter area, in the polarisations HH,VV,HV and VH.

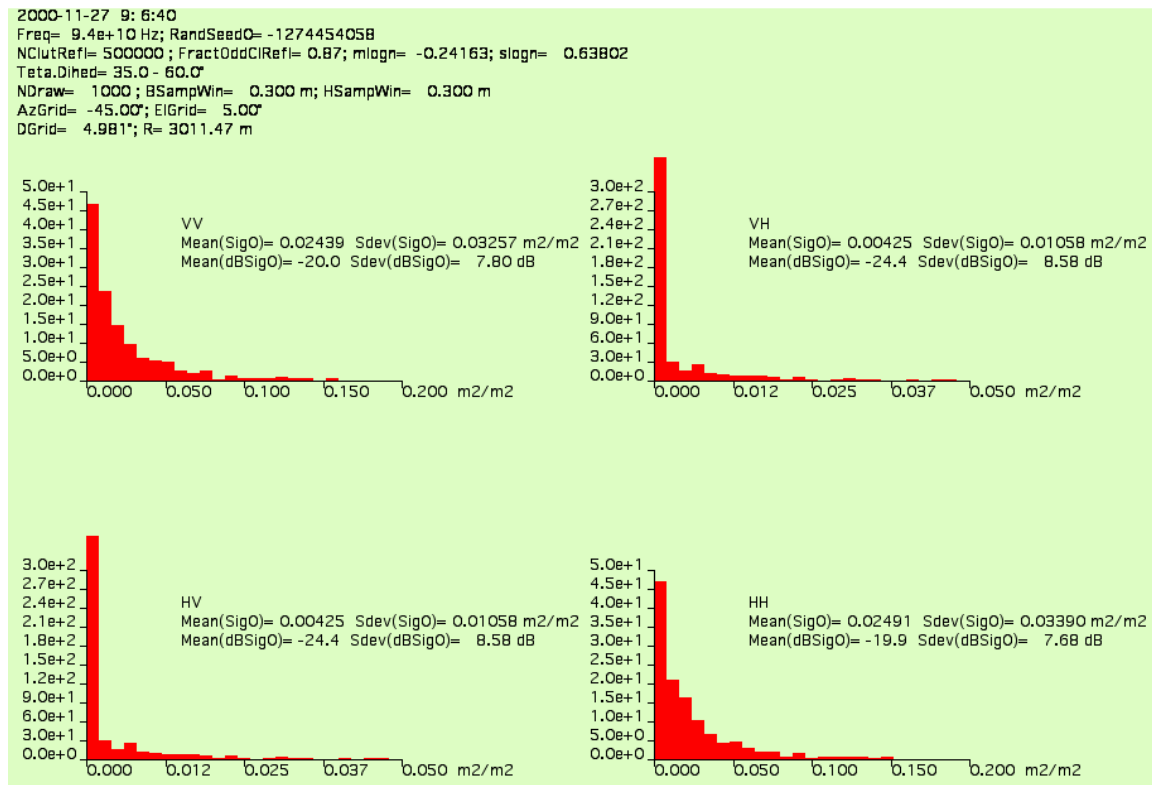


Figure 3.10 Histograms resulting from a simulated measurement with $0.3 \times 0.3 \text{ m}$ ground resolution in 1000 different directions within a clutter area about the target, from a position at 5° elevation angle and 45° from the forward direction of the target. The side of the clutter square has been taken as the cross-range footprint of the 3 dB beam of the seeker antenna with 0.15 m diameter. The number of clutter reflectors is 550000, with 86% trihedral corner reflectors. Their individual maximum radar cross sections have been drawn from a log-normal distribution with the mean $m=-0.241629$ and standard deviation $s=0.638025$; then their sizes have been adjusted with a factor to make the mean value of the reflectivity agree with the G.I.T. model. The orientations of the symmetry axes of the top-hats follow a uniform distribution, over 360° in azimuth, and over 25° in polar angle between 35° and 60° . One histogram is shown for each polarisation combination HH,VV,HV,VH, with averages and standard deviations of the reflectivity and its dB value given. The distributions display the wide tails, characteristic of clutter observed with high resolution. More values are needed for better definition of the tails.

There is a fair agreement with the adopted values for the mean, variance and cross-polarisation reflectivity from the two US sources (G.I.T. and M.I.T.). The model is valid for spatial resolutions equal to or worse than that of its construction, $0.3 \text{ m} \times 0.3 \text{ m}$. Hence, it should safely cover the case under study here, a real aperture radar where the cross-range resolution is given by the antenna beam footprint on the ground at 3 km distance, about 64 m, and where the range resolution is $\geq 0.3 \text{ m}$.

The considerable element of empirical adjustment of parameters in the fashioning of the clutter model is expected to make it less robust than the target models. The weaker physical basis will make it necessary to adjust its parameters, for instance for a significantly different elevation angle, which is not the case for the targets.

4 Simulation

4.1 Overview

Simulations have been run of target classification with two sensors, which use different levels of polarimetric information. The target set consists of the four varieties described in Section 3.3.

Briefly, the classification capability of the sensors has been calculated for a number of randomly selected azimuth positions $0-360^\circ$ about the four targets according to Figure 4.1. For each position the radar return has been calculated ("measured") in range gates along each target and compared with catalogue versions of such range profiles, determined with a specific angular increment between azimuth $0-360^\circ$. The catalogue profile providing the best fit to the measured one has given an estimate of the target type and its orientation with respect to the sensor. From a number of such trials, performance measures have been determined for a fully polarimetric sensor and a single channel system working with horizontal polarisation only.

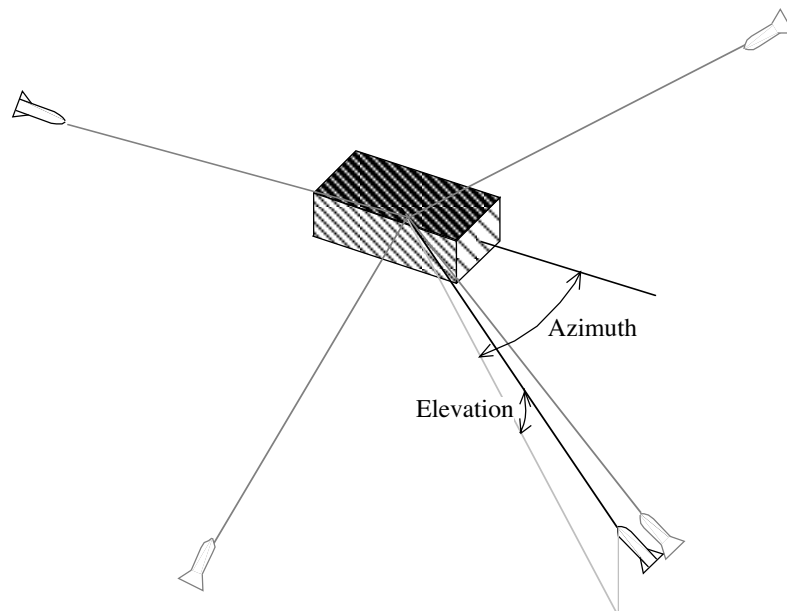


Figure 4.1 Statistics of the target discriminating capability of a sensor are generated by placing the radar in a number of randomly selected azimuth positions, $0-360^\circ$, keeping the elevation and distance constant. This is repeated for the four targets. The radar returns are compared with corresponding stored catalogue data, which gives estimates of the most probable target candidate and the azimuth angle.

4.2 System parameters

Table 4.1 lists relevant system data, with separate columns for parameters which have been kept fixed or have been varied, respectively. The sensor data have been chosen in general agreement with the system study of Karlsson *et al.* (1999), except for the specific variations as regards polarisation and range resolution.

Table 4.1 System parameters in the simulations.

| Property | Fixed | Value | Varied |
|--|---|--------------|---|
| Sensor | | | |
| Frequency | 94 GHz | | |
| Wavelength, λ | 3.2 mm | | |
| Modulation | square-wave pulse | | |
| Pulse length, τ | | | 2, 3.33, 6.67, 20 ns |
| Range resolution | | | 0.3, 0.5, 1.0, 3.0 m |
| Sampling rate, $(=1/\tau)$ | | | 500, 300, 150, 50 MHz |
| Number of range gates | | | 30, 18, 10, 4 |
| Antenna diameter, D | 0.15 m | | |
| Lobe shape | rectangular | | |
| | [1 for $0 \leq \theta \leq 1.2 \lambda/(2D)$, 0 for $\theta > 1.2 \lambda/(2D)$] | | |
| 3 dB lobe width, $1.2 \lambda/D$ | 1.5° | | |
| Aperture efficiency | 0.5 | | |
| Polarisation channels ^a | | | 1) <u>Incoherent</u> transmit H, receive H 2) <u>Fully polarimetric,</u> <u>coherent:</u> transmit H and V receive H and V |
| Target | | | |
| Shape | "box" | | |
| Dimensions (length \times width \times height) | 7.0 \times 3.6 \times 2.2 m | | |
| Type | | | 1) Tank 2) "Truck with closed platform housing" 3) "Truck with open platform" 4) Unspecified (random) |
| Geometry | | | |
| Distance target/radar | 3 km | | |
| Sensor elevation | 5° | | |
| Sensor azimuth | | | 0-360° (random) |
| Catalogue | | | |
| Azimuth increment | | | 0.01, 0.1, 1.0, 2.0, 10.0° |

^a H=Horizontal

V=Vertical

One sensor is a one-channel, incoherent system, which treats the electromagnetic field as a scalar. The other one is that of main interest in this work; it is a fully polarimetric system which measures the complete target scattering matrix, *e.g.* by switching the transmit polarisation from pulse to pulse, and with two receiving channels. One precondition for this method is that changes in the target/sensor geometry from pulse to pulse can be neglected.

The geometry is taken as static; no flight simulation has been made.

4.3 Calculation of the target echo

The monostatic radar return is calculated by coherent addition of the single reflector returns (field strengths), as shown schematically in Figure 4.2. The reflectors are approximated by point-like objects, returning spherical waves, with the far field scattering given by the

matrices in Table A.1 in the Appendix. Hence, the radar is assumed to be in the far field of the individual reflectors. (On the other hand, the radar may be located in the near field of the target as a whole).

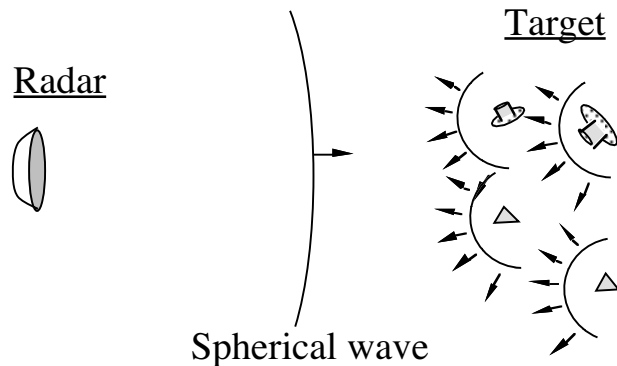


Figure 4.2 The radar return is obtained by coherently adding the returns from the single reflectors, which are assumed to produce spherical return waves (the radar is in the far field region of an individual reflector).

The horizontally and vertically polarised field strengths of the received wave are calculated for horizontal and vertical transmissions, *i.e.* the resulting scattering matrix for the reflectors found in a resolution cell of the radar is calculated, for a time (or range) sequence of sampling points. A range profile of the target is thus obtained for the different polarisation combinations. The sampling frequency can be chosen, as well as the relative positions of the sampling points with respect to the target. The arrival time of the leading edge of the radar return from the reflector closest to the radar serves as a time reference. The closest illuminated reflector is one of the four corner position markers, placed in the four upper corners of each target, as described in Section 4.3.4.1.

For each sensor position, the geometric parameters are determined which define the relative orientation between the reflectors and the radar and which are necessary for the calculation of the radar cross section: the angles δ, ψ for the cylinder hats (see Table A.1 in the Appendix) and the angle between the symmetry axis and the line of sight to the radar for the corners.

Shadowing effects and reduction of cross sections due to the orientations of the reflectors have been included. Reflectors on those sides of the targets which are not illuminated by the radar wave, viewed as rays, are given zero contribution, as are clutter reflectors on the ground in the shadow of the target (*cf.* Figure 3.9), and those reflectors where the angle δ between the symmetry axis and the line of sight to the radar is greater than 90° . In that case the reflector points away from the radar. For $0 \leq \delta \leq \pi/2$ the radar cross section of a trihedral follows a $\cos^2 \delta$ relation, whereas the reduction factor for the top-hat is $(\sin \delta / \sin 45^\circ)^2$ if $0 \leq \delta \leq \pi/4$ and $(\cos \delta / \cos 45^\circ)^2$ if $\pi/4 \leq \delta \leq \pi/2$, *cf.* Table A.1 in the Appendix. If an active part of the reflector on an illuminated surface is under the surface (*i.e.* inside the target or the ground) no reduction is assumed. Interaction between reflectors are neglected; thus the shadowing of a reflector by another is not included.

4.4 Recognition principles

4.4.1 Features

The target classification is based on a limited number (M) target features. These discriminating quantities relate to the polarisation of the radar echo. By sampling in N points

in time, chosen to cover the target in range ("range gates") a "range profile" of a feature is obtained.

4.4.1.1 Sensor with single channel

For the single channel radar, the selected feature is the squared amplitude $|s_{HH}|^2$ in the single polarisation channel (H) as a function of range, obtained as equidistant sampling points in time (range profile, Figure 4.3).

In order to focus on polarisation properties, the dependence of the classification on reflector size (radar cross section) is reduced by normalizing the feature in each range gate with the sum $|s_{HH}|^2 + |s_{HV}|^2 + |s_{VH}|^2 + |s_{VV}|^2$ of the elements in the scattering matrix of the gate. [In a real case with a single channel sensor this quantity is of course not available].

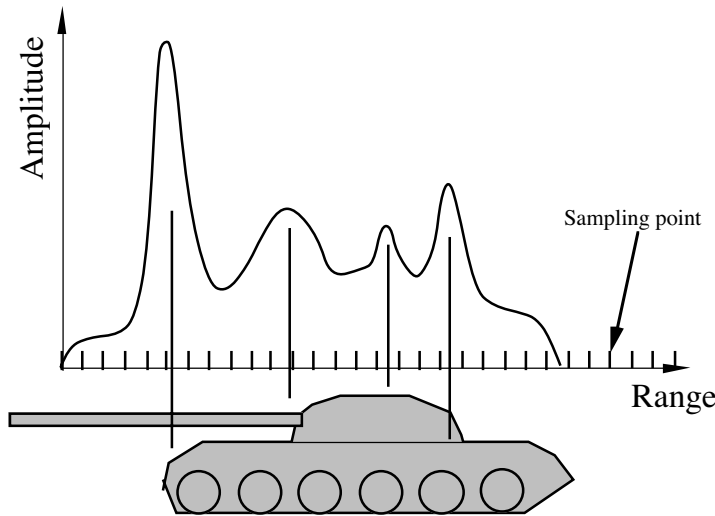


Figure 4.3 Sampled range profile determined with horizontal polarisation is the basis for classification with the single channel sensor.

4.4.1.2 Fully polarimetric coherent sensor

For the fully polarimetric sensor the features are based on the so-called Stokes' parameters of the radar return, which constitute a power-based description of the polarisation of a wave (see the Appendix, Section A.3). For the description of the transformation of these parameters through the scattering in the target, the Mueller matrix is used (see the Appendix). The elements of this matrix can be expressed with the scattering matrix coefficients $s_{HH}, s_{HV}, s_{VH}, s_{VV}$ via quadratic expressions. Huynen (1987) introduced power-based parameters, which essentially are the Mueller matrix elements, slightly rewritten. For the classification the eight Huynen parameters $A_0, B_0 + B, B_0 - B, C, D, E, F, G$ are adopted [cf. Titin-Schnaider (1998)], after a coordinate transformation which makes the ninth parameter $H = 0$. The calculation of these parameters from the scattering matrix elements is described in the Appendix, section A.4.

For the fully polarimetric sensor eight sampled range profiles are thus available for the classification, as shown in Figure 4.4. Often, it is an advantage to normalise data (*e.g.* in an uncalibrated case). The quantity $A_0 + B_0$ is used here for normalization, which can be shown to be proportional to the sum of the squares of the elements of the scattering matrix $|s_{HH}|^2 + |s_{HV}|^2 + |s_{VH}|^2 + |s_{VV}|^2$.

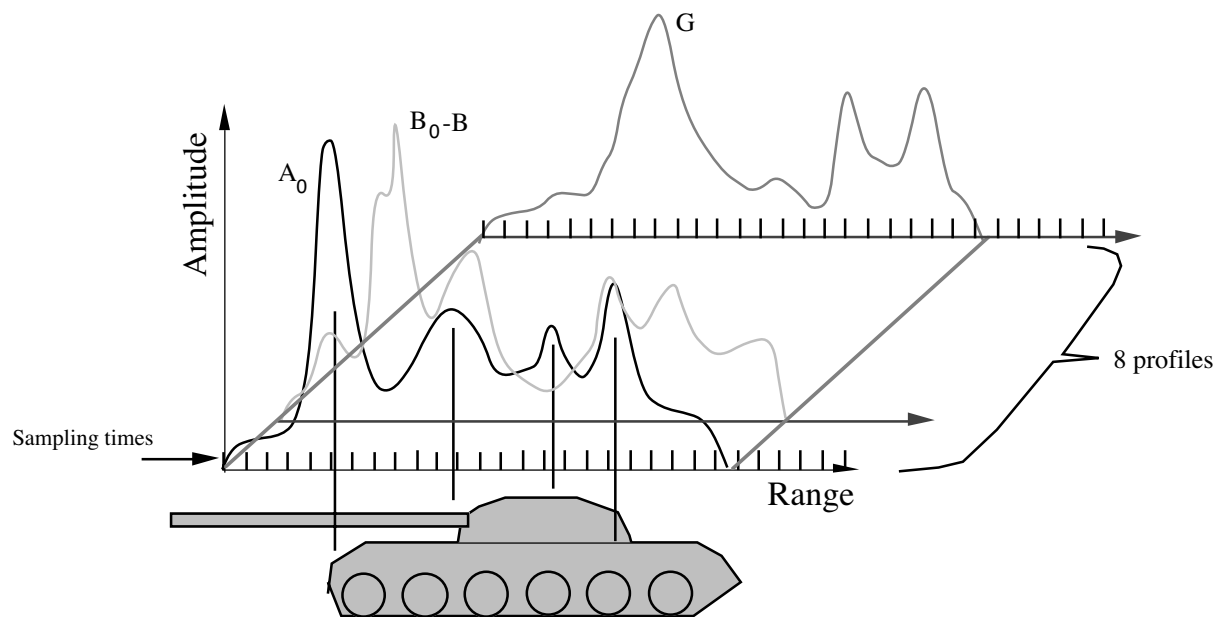


Figure 4.4 The fully polarimetric sensor uses eight parameters, based on the elements of the Mueller matrix. Eight sampled range profiles are the basis for the classification in this case.

4.4.2 Comparison with reference catalogue profiles

The target classification method chosen here is to compare measured (here: simulated) range profiles of a target (initially unknown) with stored profiles of target candidates. The method requires in a real case *a priori* knowledge of the objects so that the candidate profiles can be determined and stored in advance, for expected system parameters, *e.g.* the aspect angle.

The procedure used here is as follows. For a specific target and a specific, randomly drawn azimuth angle, a sample vector is generated, whose components are the $M \times N$ samples of the normalised features. This vector is compared with stored vectors for all four modelled targets, determined with the same system parameters, for azimuths between 0-360° in steps of ΔAz° . Five different increments in the catalogue data have been studied: $\Delta Az=0.01, 0.1, 1.0, 2.0$, and 10° , corresponding to 36000, 3600, 360, 180, and 36 azimuth values for each target in the interval 0-360°. The smallest angle step is approximately equal to the smallest angular change that gives decorrelation of the phase of the radar return for an object of the studied size. The stored vectors for the coarser steps derive from range profiles at single azimuth values, and not from averaging of data taken with a finer increment. The latter procedure would be of interest for a future study.

The choice of the most probable target candidate is made in a straightforward way: the estimated target is the one in the catalogue which has the vector with the best match with the measured one, the Euclidian distance being the matching criterion. The azimuth value of this catalogue vector defines the azimuth estimate of the observed target. Figure 4.5 illustrates the procedure.

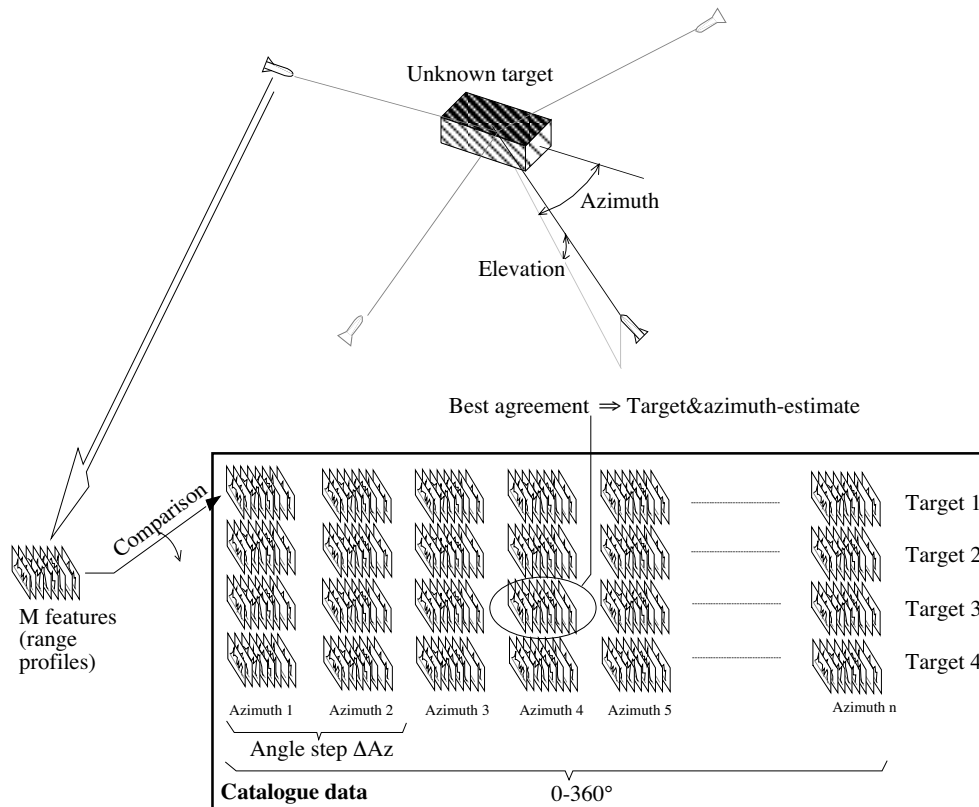


Figure 4.5 Classification principle. The radar views one of the four modelled targets from a randomly selected azimuth angle, at 5° elevation, from 3 km distance. Range profiles are calculated for the chosen polarimetric features and compared with stored catalogue data for the four possible target candidates. The closest fit gives an estimate of target type and orientation angle.

The catalogue comparison described is done for both sensor variants. Another parameter varied is the range resolution: four values $\Delta R=0.3, 0.5, 1.0$, and 3.0 m are simulated.

4.5 Computer program

The generation of targets, the calculation of the radar return and the classification is made with a computer program written in PASCAL. It is partly based on a program, generated for the previous tank modelling at the FOA (Nilsson, 1990), hence the somewhat anachronistic choice of language. The PASCAL version used is included in Metrowerks CodeWarrior Gold 11 (version 1.7.4) for Mac OS. The program has been run on a Power Mac G4, with 450 MHz clock frequency and 1 Gbyte RAM memory.

4.6 Classification performance without ground clutter

Classification performance is presented as confusion matrices showing the number of correct and false classifications of 36 simulations of each target with random selection of the azimuth angle 0-360°, i.e. one simulation in ten degrees on average. A perfectly performing sensor gives the value 36 in the diagonal positions of the matrices and zero elsewhere. The values in parentheses show the number of correct azimuth estimates, on the criterion that the azimuth

value of the catalogue profile with the smallest Euclidian distance from the measured one, is found less than 5° from the randomly selected azimuth.

Section 4.6.1 and 4.6.2 contain detailed results of the simulations, summarized in figures in Section 4.6.3, presenting probabilities of correct classification.

4.6.1 Variation of angle increment in catalogue data ($\Delta R=0.3$ m)

4.6.1.1 Angle increment 0.01°

Table 4.2 Confusion matrix with fully polarimetric sensor, $\Delta R=0.3$ m, catalogue $\Delta A_z=0.01^\circ$.

| Target | Classified as | | | |
|-------------------------|---------------|---------|---------|---------|
| | 1 | 2 | 3 | 4 |
| 1 (tank) | 35 (35) | 0 | 1 | 0 |
| 2 ("open truck") | 0 | 30 (28) | 3 | 3 |
| 3 ("closed truck") | 0 | 0 | 36 (36) | 0 |
| 4 (unspecified; random) | 0 | 2 | 2 | 32 (31) |

Table 4.3 Confusion matrix with single channel sensor (HH), $\Delta R=0.3$ m, catalogue $\Delta A_z=0.01^\circ$.

| Target | Classified as | | | |
|-------------------------|---------------|---------|---------|---------|
| | 1 | 2 | 3 | 4 |
| 1 (tank) | 27 (24) | 4 | 5 | 0 |
| 2 ("open truck") | 3 | 28 (27) | 3 | 2 |
| 3 ("closed truck") | 5 | 2 | 23 (19) | 6 |
| 4 (unspecified; random) | 3 | 0 | 4 | 29 (26) |

4.6.1.2 Angle increment 0.1°

Table 4.4 Confusion matrix with fully polarimetric sensor, $\Delta R=0.3$ m, catalogue $\Delta A_z=0.1^\circ$.

| Target | Classified as | | | |
|-------------------------|---------------|---------|---------|---------|
| | 1 | 2 | 3 | 4 |
| 1 (tank) | 33 (31) | 0 | 3 | 0 |
| 2 ("open truck") | 0 | 29 (25) | 4 | 3 |
| 3 ("closed truck") | 0 | 4 | 29 (21) | 3 |
| 4 (unspecified; random) | 1 | 2 | 2 | 31 (29) |

Table 4.5 Confusion matrix with single channel sensor (HH), $\Delta R=0.3$ m, catalogue $\Delta A_z=0.1^\circ$.

| Target | Classified as | | | |
|-------------------------|---------------|---------|--------|---------|
| | 1 | 2 | 3 | 4 |
| 1 (tank) | 17 (8) | 3 | 14 | 2 |
| 2 ("open truck") | 6 | 19 (14) | 6 | 5 |
| 3 ("closed truck") | 6 | 6 | 14 (8) | 10 |
| 4 (unspecified; random) | 6 | 4 | 10 | 16 (12) |

4.6.1.3 Angle increment 1.0°

Table 4.6 Confusion matrix with fully polarimetric sensor, $\Delta R=0.3$ m, catalogue $\Delta A_z=1.0^\circ$.

| Target | Classified as | | | |
|-------------------------|---------------|---------|---------|---------|
| | 1 | 2 | 3 | 4 |
| 1 (tank) | 23 (19) | 3 | 7 | 3 |
| 2 ("open truck") | 2 | 21 (14) | 8 | 5 |
| 3 ("closed truck") | 1 | 10 | 21 (14) | 4 |
| 4 (unspecified; random) | 2 | 5 | 5 | 24 (18) |

Table 4.7 Confusion matrix with single channel sensor (HH), $\Delta R=0.3$ m, catalogue $\Delta A_z=1.0^\circ$.

| Target | Classified as | | | |
|-------------------------|---------------|--------|-------|--------|
| | 1 | 2 | 3 | 4 |
| 1 (tank) | 13 (5) | 5 | 13 | 5 |
| 2 ("open truck") | 8 | 15 (9) | 4 | 9 |
| 3 ("closed truck") | 16 | 5 | 9 (4) | 6 |
| 4 (unspecified; random) | 7 | 6 | 10 | 13 (4) |

4.6.1.4 Angle increment 2.0°

Table 4.8 Confusion matrix with fully polarimetric sensor, $\Delta R=0.3$ m, catalogue $\Delta A_z=2.0^\circ$.

| Target | Classified as | | | |
|-------------------------|---------------|---------|---------|---------|
| | 1 | 2 | 3 | 4 |
| 1 (tank) | 25 (17) | 3 | 5 | 3 |
| 2 ("open truck") | 0 | 17 (15) | 16 | 3 |
| 3 ("closed truck") | 2 | 5 | 25 (17) | 4 |
| 4 (unspecified; random) | 4 | 4 | 6 | 22 (16) |

Table 4.9 Confusion matrix with single channel sensor (HH), $\Delta R=0.3$ m, catalogue $\Delta A_z=2.0^\circ$.

| Target | Classified as | | | |
|-------------------------|---------------|--------|--------|--------|
| | 1 | 2 | 3 | 4 |
| 1 (tank) | 21 (2) | 4 | 5 | 6 |
| 2 ("open truck") | 5 | 16 (7) | 6 | 9 |
| 3 ("closed truck") | 12 | 3 | 13 (2) | 8 |
| 4 (unspecified; random) | 6 | 4 | 11 | 15 (5) |

4.6.1.5 Angle increment 10°

Table 4.10 Confusion matrix with fully polarimetric sensor, $\Delta R=0.3$ m, catalogue $\Delta A_z=10.0^\circ$.

| Target | Classified as | | | |
|-------------------------|---------------|-------|--------|--------|
| | 1 | 2 | 3 | 4 |
| 1 (tank) | 21 (14) | 1 | 3 | 11 |
| 2 ("open truck") | 2 | 8 (5) | 13 | 13 |
| 3 ("closed truck") | 7 | 3 | 12 (8) | 14 |
| 4 (unspecified; random) | 8 | 5 | 9 | 14 (5) |

Table 4.11 Confusion matrix with single channel sensor (HH), $\Delta R=0.3$ m, catalogue $\Delta A_z=10.0^\circ$.

| Target | Classified as | | | |
|-------------------------|---------------|-------|--------|-------|
| | 1 | 2 | 3 | 4 |
| 1 (tank) | 16 (0) | 2 | 12 | 6 |
| 2 ("open truck") | 10 | 9 (2) | 8 | 9 |
| 3 ("closed truck") | 10 | 4 | 15 (2) | 7 |
| 4 (unspecified; random) | 7 | 5 | 15 | 9 (1) |

4.6.2 Variation of range resolution ($\Delta A_z=0.1^\circ$)

4.6.2.1 Range resolution 0.3 m

Table 4.12 Confusion matrix with fully polarimetric sensor, $\Delta R=0.3$ m, catalogue $\Delta A_z=0.1^\circ$.

| Target | Classified as | | | |
|-------------------------|---------------|---------|---------|---------|
| | 1 | 2 | 3 | 4 |
| 1 (tank) | 33 (31) | 0 | 3 | 0 |
| 2 ("open truck") | 0 | 29 (25) | 4 | 3 |
| 3 ("closed truck") | 0 | 4 | 29 (21) | 3 |
| 4 (unspecified; random) | 1 | 2 | 2 | 31 (29) |

Table 4.13 Confusion matrix with single channel sensor (HH), $\Delta R=0.3$ m, catalogue $\Delta A_z=0.1^\circ$.

| Target | Classified as | | | |
|-------------------------|---------------|---------|--------|---------|
| | 1 | 2 | 3 | 4 |
| 1 (tank) | 17 (8) | 3 | 14 | 2 |
| 2 ("open truck") | 6 | 19 (14) | 6 | 5 |
| 3 ("closed truck") | 6 | 6 | 14 (8) | 10 |
| 4 (unspecified; random) | 6 | 4 | 10 | 16 (12) |

4.6.2.2 Range resolution 0.5 m

Table 4.14 Confusion matrix with fully polarimetric sensor, $\Delta R=0.5$ m, catalogue $\Delta A_z=0.1^\circ$.

| Target | Classified as | | | |
|-------------------------|---------------|---------|---------|---------|
| | 1 | 2 | 3 | 4 |
| 1 (tank) | 24 (23) | 4 | 6 | 2 |
| 2 ("open truck") | 3 | 17 (15) | 6 | 10 |
| 3 ("closed truck") | 2 | 2 | 29 (23) | 3 |
| 4 (unspecified; random) | 6 | 1 | 5 | 24 (18) |

Table 4.15 Confusion matrix with single channel sensor (HH), $\Delta R=0.5$ m, catalogue $\Delta A_z=0.1^\circ$.

| Target | Classified as | | | |
|-------------------------|---------------|--------|--------|--------|
| | 1 | 2 | 3 | 4 |
| 1 (tank) | 11 (5) | 6 | 10 | 9 |
| 2 ("open truck") | 8 | 16 (7) | 5 | 7 |
| 3 ("closed truck") | 3 | 9 | 13 (6) | 11 |
| 4 (unspecified; random) | 6 | 5 | 12 | 13 (7) |

4.6.2.3 Range resolution 1.0 m

Table 4.16 Confusion matrix with fully polarimetric sensor, $\Delta R=1.0$ m, catalogue $\Delta A_z=0.1^\circ$.

| Target | Classified as | | | |
|-------------------------|---------------|---------|---------|-------|
| | 1 | 2 | 3 | 4 |
| 1 (tank) | 17 (10) | 4 | 6 | 9 |
| 2 ("open truck") | 4 | 19 (12) | 4 | 9 |
| 3 ("closed truck") | 2 | 8 | 22 (12) | 4 |
| 4 (unspecified; random) | 14 | 5 | 8 | 9 (2) |

Table 4.17 Confusion matrix with single channel sensor (HH), $\Delta R=1.0$ m, catalogue $\Delta A_z=0.1^\circ$.

| Target | Classified as | | | |
|-------------------------|---------------|--------|-------|--------|
| | 1 | 2 | 3 | 4 |
| 1 (tank) | 9 (2) | 5 | 11 | 11 |
| 2 ("open truck") | 7 | 11 (2) | 4 | 14 |
| 3 ("closed truck") | 13 | 11 | 7 (1) | 5 |
| 4 (unspecified; random) | 10 | 7 | 6 | 13 (1) |

4.6.2.4 Range resolution 3.0 m

Table 4.18 Confusion matrix with fully polarimetric sensor, $\Delta R=3.0$ m, catalogue $\Delta A_z=0.1^\circ$.

| Target | Classified as | | | |
|-------------------------|---------------|--------|-------|--------|
| | 1 | 2 | 3 | 4 |
| 1 (tank) | 12 (3) | 6 | 9 | 9 |
| 2 ("open truck") | 3 | 15 (1) | 7 | 11 |
| 3 ("closed truck") | 10 | 4 | 9 (1) | 13 |
| 4 (unspecified; random) | 1 | 13 | 8 | 14 (1) |

Table 4.19 Confusion matrix with single channel sensor (HH), $\Delta R=3.0$ m, catalogue $\Delta A_z=0.1^\circ$.

| Target | Classified as | | | |
|-------------------------|---------------|--------|-------|-------|
| | 1 | 2 | 3 | 4 |
| 1 (tank) | 16 (0) | 9 | 3 | 8 |
| 2 ("open truck") | 9 | 12 (0) | 7 | 8 |
| 3 ("closed truck") | 12 | 7 | 8 (1) | 9 |
| 4 (unspecified; random) | 3 | 17 | 7 | 9 (0) |

4.6.3 Probabilities of correct classification

From the above tables, probabilities of correct classification can be calculated. Table 4.20 shows the dependence on the angle increment in catalogue data, with fixed range resolution $\Delta R=0.3$ m. Table 4.21 lists the performance when the range resolution is varied, with fixed catalogue angle increment $\Delta A_z=0.1^\circ$. The values for the four targets are similar enough to warrant an averaging, the result of which is shown on the bottom lines in the tables and which is plotted as curves in Figure 4.6 and 4.7.

Table 4.20 Probabilities of correct classification for varying angle step in catalogue, with range resolution $\Delta R=0.3$ m.

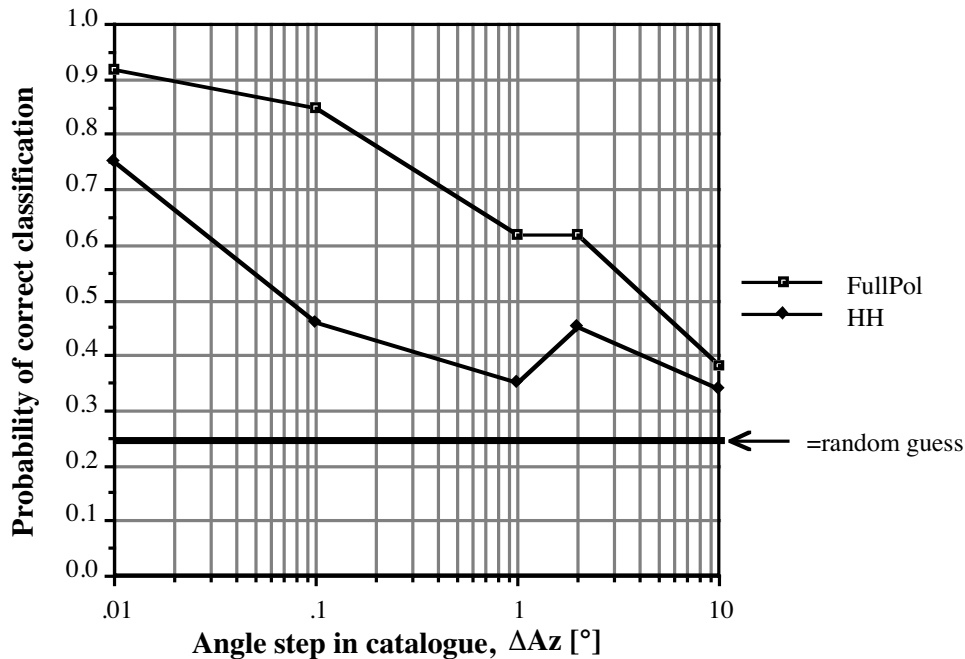
| Target | Angle step in catalogue [°] | | | | | | | | | |
|--------|-----------------------------|-----------------|------|------|------|------|------|------|------|------|
| | 0.01 | | 0.1 | | 1.0 | | 2.0 | | 10.0 | |
| | Fpol ^a | HH ^a | Fpol | HH | Fpol | HH | Fpol | HH | Fpol | HH |
| 1 | 0.97 | 0.75 | 0.92 | 0.47 | 0.64 | 0.36 | 0.69 | 0.58 | 0.58 | 0.44 |
| 2 | 0.83 | 0.78 | 0.81 | 0.53 | 0.58 | 0.42 | 0.47 | 0.44 | 0.22 | 0.25 |
| 3 | 1.00 | 0.64 | 0.81 | 0.39 | 0.58 | 0.25 | 0.69 | 0.36 | 0.33 | 0.42 |
| 4 | 0.89 | 0.80 | 0.86 | 0.44 | 0.67 | 0.36 | 0.61 | 0.42 | 0.39 | 0.25 |
| Mean | 0.92 | 0.75 | 0.85 | 0.46 | 0.62 | 0.35 | 0.62 | 0.45 | 0.38 | 0.34 |

^a Fpol=Fully polarimetric system; HH=Single channel system with horizontal polarisation

Table 4.21 Probabilities of correct classification for varying range resolution, with angle step in catalogue $\Delta Az = 0.1^\circ$.

| Target | Range resolution [m] | | | | | | | |
|--------|----------------------|-----------------|------|------|------|------|------|------|
| | 0.3 | | 0.5 | | 1.0 | | 3.0 | |
| | Fpol ^a | HH ^a | Fpol | HH | Fpol | HH | Fpol | HH |
| 1 | 0.92 | 0.47 | 0.67 | 0.31 | 0.47 | 0.25 | 0.33 | 0.44 |
| 2 | 0.81 | 0.53 | 0.47 | 0.44 | 0.53 | 0.31 | 0.42 | 0.33 |
| 3 | 0.81 | 0.39 | 0.81 | 0.36 | 0.61 | 0.19 | 0.25 | 0.22 |
| 4 | 0.86 | 0.44 | 0.67 | 0.36 | 0.25 | 0.36 | 0.39 | 0.25 |
| Mean | 0.85 | 0.46 | 0.66 | 0.37 | 0.47 | 0.28 | 0.35 | 0.31 |

^a Fpol=Fully polarimetric system; HH=Single channel system with horizontal polarisation



Figur 4.6 Mean values over the four targets, of the probability of correct classification as a function of angle increment in the reference catalogue, for a fully polarimetric system (upper curve) and for a single channel system with horizontal polarisation. Random guessing gives the value 1/4, as shown. The range resolution is $\Delta R = 0.3$ m.

As seen from Figure 4.6, in order to obtain a probability of correct classification of about 90%, firstly, the sensor must be fully polarimetric, and secondly, the reference data must be catalogued with less than 0.1° increment. The single channel system has a performance lying some tens of percent below that of the fully polarimetric one.

A marked sensitivity to the range resolution is displayed in Figure 4.7. At least the nominal value $\Delta R = 0.3$ m is required if the performance of 90% correct classification is to be reached with the fully polarimetric system, with an assumed spacing $\Delta Az = 0.1^\circ$ of reference data. The single channel system shows considerably worse performance.

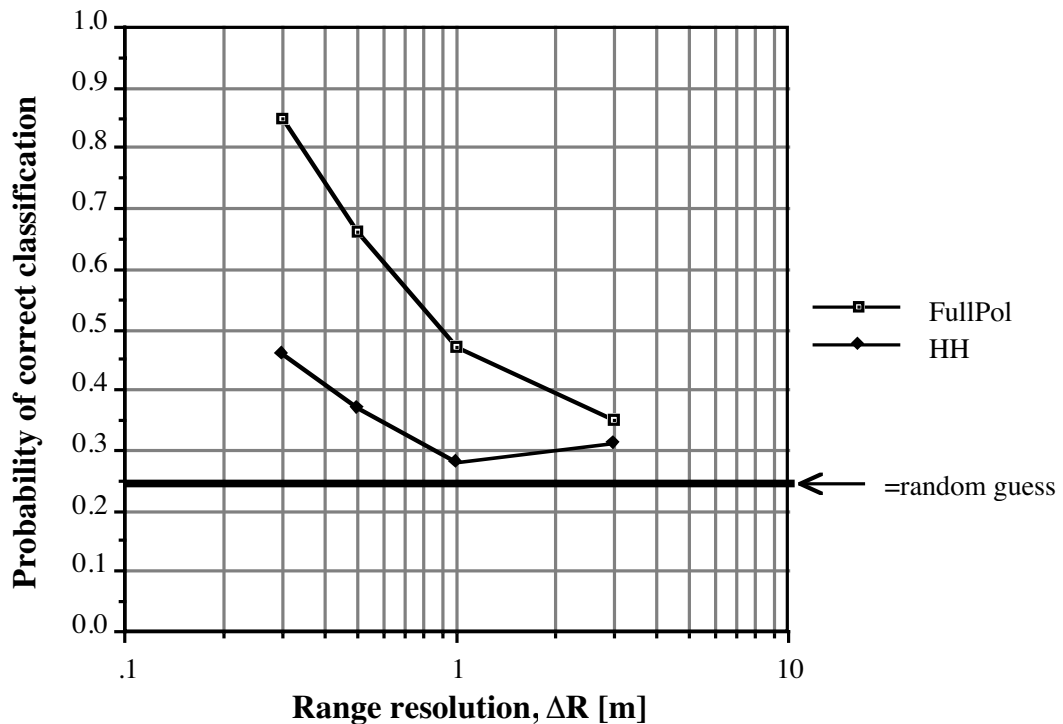


Figure 4.7 Mean values of the probability of correct classification of the four targets as a function of range resolution, for a fully polarimetric system (upper curve) and for a single-channel system with horizontal polarisation. Random guessing gives the value $1/4$, as shown. A reference catalogue with 0.1° angle step between data is assumed. [As discussed in the text the abscissa scale can be taken to represent the range resolution normalised with the mean nominal distance between the reflectors on the target surfaces, which is approximately 1 m.]

4.6.4 Resolution and reflector separation

There is reason for trying to relate the abscissa in figure 4.7 to target structure (normalization), since successful recognition is presumed to correlate with the ability of the sensor to isolate single reflectors in range cells for polarimetric analysis. The range resolution of the radar should thus be seen in relation to the separation between the reflectors along the line of sight. The appearance of many reflectors in a range gate will make recognition difficult, which may be alleviated with an improvement of the range resolution. On the other hand, there is little sense in using a resolution so high that there are no reflectors in a significant number of range gates along the target. The cross range distribution also has to be considered in a similar fashion. Generally, the number of reflectors in the individual gates is dependent on the aspect angle as well, and so will be the prospect of successful recognition. A good understanding of these matters requires a detailed investigation for individual azimuths and targets. This will not be pursued here to full extent, but we will give some illustrations, with various standard of precision.

In view of the above discussion, it is difficult to find a simple, universal quantity that relates the sensor resolution to target structure. Taking a coarse view to begin with, an aspect independent nominal figure that represents the mean distance between the reflectors on one rectangular side of a target is obtained by taking the square root of the ratio between the surface area and the number of reflectors on that area. The targets are enough similar to make an averaging over the surfaces of all four targets meaningful; one obtains the value $\Delta s = 0.92$ m for this average. Since the value is close to 1 m, one can within the approximation

uncertainties take the abscissa values in Figure 4.7 to represent the normalised range resolution $\Delta R / \Delta s$.

A more precise representation is given by the number of reflectors that for a specific azimuth value actually occur in the individual range gates, and that are located and oriented to contribute to the radar return. Table 4.22 shows the average of these numbers, where a threefold averaging has been made: (1) over the range gates that span the target, (2) over the 36 randomly drawn azimuths, and (3) over the four targets. This has been done for each individual range resolution ΔR , as given in the table. One can see from the table that the calculated mean is closely proportional to the range resolution, so the abscissa scale in figure 4.7 multiplied with $\approx 20/3$ can be taken to represent this mean.

Table 4.22 *Mean number of contributing reflectors per range gate, taken over gates spanning the target, over 36 randomly generated azimuths and over the four targets.*

| Mean number of reflectors per range gate | | | |
|--|----------------|----------------|--------------------|
| $\Delta R=0.3$ | $\Delta R=0.5$ | $\Delta R=1.0$ | $\Delta R=3.0$ [m] |
| 2.0 | 3.3 | 6.5 | 20.1 |

A still more detailed view, involving no averaging, is shown in Figure 4.8, which depicts how the contributing reflectors are distributed in the individual range gates, for specific azimuth angles and for a specific target. The example in the figure refers to the tank target, observed with $\Delta R=0.3$ m resolution in the 36 randomly drawn azimuth positions between 0-360°. The bars represent the number of contributing reflectors in the individual range gates along the target. One can see that typically this number varies between 0 and about 5, with marked increase for aspects where a surface is seen almost perpendicularly (e.g. $\approx 270^\circ$). The general impression is that there are many gates with a single-reflector polarisation signature, which should be conducive to successful classification.

To sum up the main result of Figure 4.7 in the light of these elaborations, the outcome of the classification is very sensitive to range resolution. For acceptable performance, the range resolution must not exceed the distance between the reflectors in the targets: with our models, to achieve 90% probability of correct classification, the range resolution should be about 25% of the nominal reflector separation (defined above). Intuitively, the best situation for unambiguous reflector identification can be expected to occur with a single reflector in a range gate. The result is also in agreement with the experimental and theoretical work by the M.I.T. group of target identification with an airborne 35 GHz SAR: Novak *et al.* (1996) state, comparing the performances of two systems with 0.3×0.3 m and 1×1 m ground resolution, respectively, that it is very difficult to perform classification with 1×1 m resolution data.⁷

⁷ It should be mentioned that polarisation is only one of the discrimination features used in the M.I.T. automatic target recognition system.

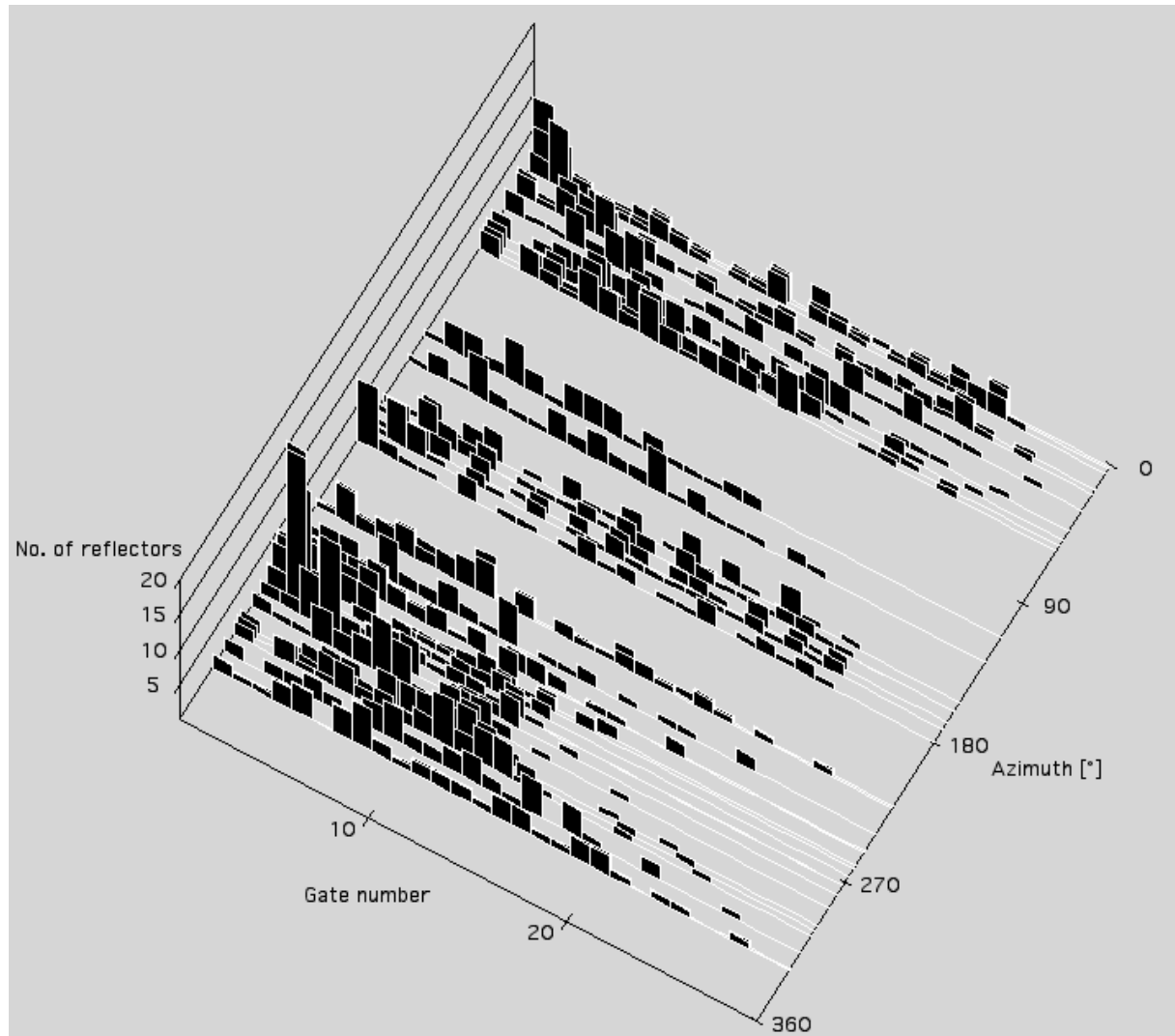


Figure 4.8 Range profiles of the tank target, with bars showing the number of reflectors contributing to the radar return from the individual range gates, for 36 randomly drawn azimuths.

4.7 Performance with clutter

Simulations with clutter, modelled as described in Section 3.4, show severe deterioration of the classification capability of the sensors, using the same principles as in the clutter-free case. However, the uncertainties in these findings are considerable. The result is dependent on correct relative strengths between the target and clutter returns. Many parameters for both the clutter and the targets are more or less postulated, with little experimental backing for the same system parameters. Hence, it is premature to draw detailed quantitative conclusions from the obtained results. However, it is safe to say that there is a general need for clutter reduction, in scenarios of the studied type. Methods at hand include Doppler filtering of moving targets, SAR technique for radical increase of cross range resolution, and more sophisticated signal processing methods using advance knowledge of targets and clutter, as used in the M.I.T. SAR work for example (Dudgeon and Lacoss, 1993).

5 Experiment

An experimental demonstration has been carried out of the feasibility to recognize, by polarimetric methods, single reflectors of the kind used as building blocks in the modelling. The experiment is in congruence with the thinking behind the recognition, in which it is assumed that by using high spatial resolution, single reflectors of simple kind can be isolated in a resolution cell, and classified. Recognition of the whole target is based on the combination of such deductions. If the basic single-reflector recognition turns out to be unfeasible in practice, one can hardly hope to succeed in the overall task.

An account of the equipment and the measurements, including calibration, is given by Johansson and Sume (2001). Here, we first give a short overview of these items and then use the data in the recognition demonstration in the next section.

5.1 Reflector measurements

The measurements were made using a coherent 94 GHz fully polarimetric, monostatic, pulsed radar. Some of its relevant characteristics are given in Table 5.1. The radar is intended for field measurements of stationary targets.

Table 5.1 Radar characteristics

| | |
|----------------------|---------------|
| Frequency | 94.0 GHz |
| Transmitter | Pulsed Impatt |
| Pulse length | 130 ns |
| Antenna | Cassegrain |
| Antenna diameter | 0.46 m |
| Polarisation | |
| Transmit (1 channel) | H,V (switch) |
| Receive (2 channels) | H,V |

The measurements were made outdoors on the roof of the FOI building at Linköping presenting a setting which was relatively well-controlled, but not dedicated for radar measurements like a test-range. The scattering matrices of a number of reflectors were determined. These were of four types: (1) circular flat plate, (2) trihedral corner reflector with orthogonal, triangular sides, (3) dihedral corner reflector with orthogonal, rectangular sides, and (4) top-hat sector consisting of two orthogonal surfaces, one planar and one forming part of a cylinder mantle (the reflector is sometimes called "Bruderhedral" in the literature). This reflector has approximately the same scattering matrix as the cylinder hat, within properly chosen aspect angle limits (Currie and Currie, 1987). The two latter types were oriented in three ways, forming $\psi = 0, 22.5^\circ$ and 45° , respectively, with the horizontal, as defined in Figure 5.1.

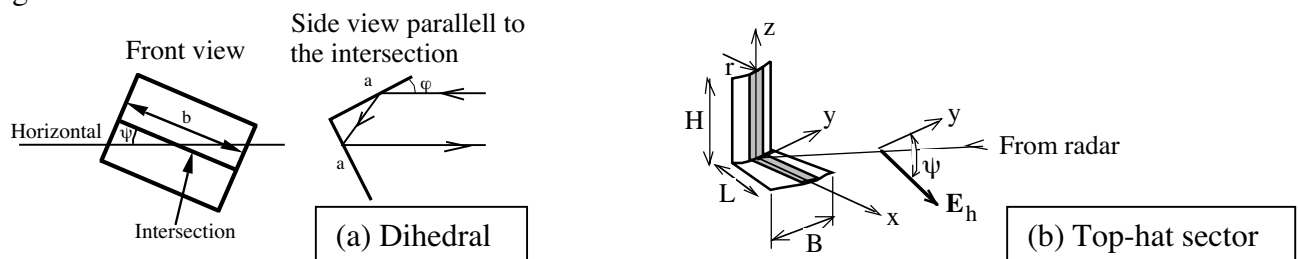


Figure 5.1 Dihedral and top-hat sector, with quantities for specification of orientation and size. At right, \mathbf{E}_h denotes the horizontal component of the electric field of the incident wave.

Table 5.2 lists the reflectors measured, including those used for the calibration.

Table 5.2 *The reflectors*

| Reflector type | Nominal radar cross section (hf-approximation) [m ²] | Characteristic dimensions ^a [m] | Remark |
|---------------------|---|--|-------------|
| Circular flat plate | 1 | $D_1=0.0338$ | Calibration |
| | 10 | $D_1=0.0602$ | |
| | 100 | $D_1=0.107$ | |
| | | | |
| Trihedral | 1 | $L=0.0395$ | |
| | 10 | $L=0.0702$ | |
| | 50 | $L=0.1050$ | |
| | 100 | $L=0.1248$ | |
| | 200 | $L=0.1485$ | |
| Plane dihedral | 50 | $a=0.05623$; $b=0.08$ | Calibration |
| | 100 | $a=0.06362$; $b=0.10$ | |
| | 556 | $a=0.10$; $b=0.15$ | |
| Hat sector | 10 | $r=0.18$; $H=L=0.1$; $B=0.193$ | |
| | 50 | $r=0.63$; $H=L=0.12$; $B=0.238$ | |
| | 100 | $r=0.80$; $H=L=0.15$; $B=0.261$ | |

^a D_1 = plate diameter. L = length of intersection between sides. The other quantities are defined in fig. 5.1.

One by one, the reflectors were measured while mounted on a turntable as shown in Figure 5.2. Usual attention was paid to multipath and other effects known to influence this type of measurements (see Johansson and Sume, 2001).



Figure 5.2 Turntable with support, holding hat-sector-type reflector.

For obtaining the scattering matrices of the reflectors, the polarisation properties of the radar itself was determined from a calibration procedure described by Brock (1991), including one trihedral and two dihedral measurements. In the latter the dihedrals are oriented with $\psi = 0^\circ$ and 22.5° , respectively, with respect to the horizontal. From these measurements the polarisation distortion of the radar can be determined; no assumption of reciprocity is made, or that the distortions in the receiver and transmitter parts are equal. The radar returns from the reflectors in the recognition measurements could then be corrected for the distortion, producing 23 scattering matrices of objects treated as unknown. These matrices served as input to the recognition exercise.

5.2 Polarimetric recognition

Recognition, in the sense used here, implies a choice of reflector type from a canonical set. In order to make it a little more than choosing between the two basic varieties figuring in the measurement, *i.e.* "even" and "odd" bounce (section 3.2), a set of eight reflector types has been created, adopted from the work of Cameron and Leung (1992). The types are listed in Table 5.3, with scattering matrices with normalizations and absolute phases as defined by Cameron and Leung. [These latter quantities disappear in the following step.]

Table 5.3 *Set of possible scatterers in the recognition task*

| Type | Scattering matrix |
|-----------------------------------|--|
| Trihedral (& flat plate & sphere) | $\frac{1}{\sqrt{2}} \begin{pmatrix} 1 & 0 \\ 0 & 1 \end{pmatrix}$ |
| Dihedral (& hat sector) | $\frac{1}{\sqrt{2}} \begin{pmatrix} 1 & 0 \\ 0 & -1 \end{pmatrix}$ |
| Dipole | $\begin{pmatrix} 1 & 0 \\ 0 & 0 \end{pmatrix}$ |
| Cylinder | $\frac{1}{\sqrt{5}} \begin{pmatrix} 2 & 0 \\ 0 & 1 \end{pmatrix}$ |
| Narrow dihedral | $\frac{1}{\sqrt{5}} \begin{pmatrix} 2 & 0 \\ 0 & -1 \end{pmatrix}$ |
| Quarter-wave device | $\frac{1}{\sqrt{2}} \begin{pmatrix} 1 & 0 \\ 0 & i \end{pmatrix}$ |
| Left hand helix | $\frac{1}{2} \begin{pmatrix} 1 & i \\ i & -1 \end{pmatrix}$ |
| Right hand helix | $\frac{1}{2} \begin{pmatrix} 1 & -i \\ -i & -1 \end{pmatrix}$ |

As in section 4.4 the recognition is based upon a feature vector, whose components are the $M = 8$ Huynen parameters $A_0, B_0 + B, B_0 - B, C, D, E, F, G$, calculated from the scattering matrices as described in the Appendix, section A.4. Since the radar cross section (RCS) is not chosen as a feature in this experiment, the Huynen parameters are normalised, with $A_0 + B_0$ as in section 4.4.

For each of the 23 reflectors, the measured Huynen parameters are compared with those of the canonical reflectors. The type estimate is taken as the canonical reflector that has a feature vector being closest to the corresponding measured vector, in the Euclidian sense. Furthermore, the ψ angle of the maximum polarisation (Appendix A.3.2) is calculated, if the reflector is classified as a dihedral (including top-hat sector). This angle equals the orientation angle of the reflector as defined in Figure 5.1. It is ambiguous with $n\frac{\pi}{2}$ (Appendix, section A.4.3.1). For the trihedral types, where the scattering matrix is independent of the roll orientation, there is no corresponding ψ -angle with geometrical significance.

Table 5.4 lists the result of the classification and the determination of the orientation ψ (dihedrals and top-hat sectors).

Table 5.4 Result of reflector recognition

| Real reflector | | | Estimate from polarimetric radar return | |
|----------------|--------------------------|---|---|-----------------------------|
| Type | RCS [m ²] | Roll orientation ψ [°] measured with clinometer | Canonical type | Roll orientation ψ [°] |
| Flat plate | 1 | - | Sphere | - |
| --" | 10 | - | Sphere | - |
| Trihedral | 1 | - | Sphere | - |
| --" | 10 | - | Sphere | - |
| --" | 50 | - | Sphere | - |
| --" | 100 | - | Sphere | - |
| --" | 200 | - | Sphere | - |
| Dihedral | 50 | 0 | Dihedral | -0.9 |
| --" | " | 22.5 | Dihedral | 21.3 |
| --" | " | 45 | Dihedral | 43.6 |
| --" | 100 | 45 | Dihedral | 44.2 |
| --" | 556 | 0 | Dihedral | 0.2 |
| --" | " | 22.5 | Dihedral | 22.0 |
| --" | " | 45 | Dihedral | 44.3 |
| Hat sector | 10 | 0 | Dihedral | 2.5 |
| --" | " | 22.5 | Dihedral | 24.2 |
| --" | " | 45 | Dihedral | 46.6 |
| --" | 50 | 0 | Dihedral | 1.0 |
| --" | " | 22.5 | Dihedral | 23.0 |
| --" | " | 45 | Dihedral | 45.5 |
| --" | 100 | 0 | Dihedral | 0.6 |
| --" | " | 22.5 | Dihedral | 25.0 |
| --" | " | 45 | Dihedral | 45.9 |

The result of the polarimetric recognition is that the choice of type, from the canonic set in Table 5.3, is made with no error by the algorithm (of course, there is no discrimination between different reflectors, having the same scattering matrix, *e.g.* between a sphere, trihedral and a plat plate). In no case is a reflector of a different canonical type chosen. The orientation angle of the dihedrals and hat-sectors is determined with an accuracy of the

order of 1°; for the flat-sided dihedrals, the accuracy is of the same order as that of the independent measurement, which was made with a spirit-level ("clinometer").

It should be emphasized that a necessary condition for succeeding with the polarimetric recognition is that the polarimetric properties of the radar are accurately known, *e.g.* through the calibration. However, the radar need not be perfect as regards polarisation purity or low polarisation distortion. The radar used was far from ideal in these respects. It was found that if a simpler calibration procedure was followed to establish the polarimetric distortion of the system, using only a single calibration reflector, a considerable error rate occurred in the classification, accompanied by a corresponding failure or increased inaccuracy in determining ψ .

6 Summary and conclusions

The main purpose of this work has been to illustrate what improvement can be brought about by using the polarisation of a radar wave for target classification in a mm-wave seeker at 94 GHz, operating in an air-to-ground missile. In the application considered for the IRmm Multisensor project the seeker radar teams with an IR sensor. The present work focuses on the radar channel by studying its properties alone, by modelling, simulation, and experiment.

A computer program that generates polarimetric models of four targets and of ground clutter (grass) has been developed. The scattering objects are made up of two types of discrete reflectors, *viz.* a right-angle corner and a cylinder hat reflector. The target reflectors are distributed over rectangular, plane surfaces, to form the outer contours of box-shaped objects. The reflector parameters (type, number, orientation, position, and size) are chosen differently for the four model objects. One of these is intended to represent the main target and is built on earlier modelling at the FOA of a tank (Centurion), which was partly based on measurements at 94 GHz. A further three targets have been generated for the study of the discriminating ability of the seeker. They are not derived directly from measured radar signatures but should be seen as more fictive creations. Two are intended to represent trucks of somewhat different design and are based on eye-inspection of a real object and of ISAR images of similar targets, whereas one is unspecified and has been generated by partly random parameter choice. The targets are all of a size, in order to concentrate the work on classification using polarimetric discriminators only. The ground clutter has been generated with a large number (up to 600000) small reflectors of the two types. The target models are valid for arbitrary sensor positions in the upper hemisphere, whereas the clutter is modelled for 5° elevation angle, but arbitrary azimuth.

Simulations of target classification have been made using two different sensors: (a) a non-coherent, single channel system with horizontal polarisation, (b) a coherent system that measures the complete scattering matrix. For each sensor four different range resolutions are examined, *viz.* 0.3, 0.5, 1.0 and 3.0 m. The systems are of real aperture type, with 0.15 m antenna diameters.

The sensors have been placed at 3 km distance from the targets. Statistics of classification performance have been generated by random selection of sensor positions 0-360° in azimuth, keeping the elevation constant at 5°. The geometry is taken as static; no flight simulation has been made.

The classification is made on the basis of a number of features, calculated from the time-sampled radar return from a target (range profiles). The features are based on the so-called Huynen parameters for the fully polarimetric sensor. These parameters are power-based quantities, which can be calculated from quadratic combinations of the measured scattering matrix elements. For the single-channel sensor the sampled amplitude in the only polarisation (horizontal) is used.

The time- (or distance-)sampled features are collected in sample vectors which are compared with stored vectors for all four targets at azimuths between 0-360°. Five different angle increments in the catalogue data have been studied, *viz.* 0.01, 0.1, 1, 2, and 10°. The choice of the most probable target candidate is made simply by selecting that catalogue target which has the vector with the smallest Euclidian distance to the measured (=simulated) one.

Classification performance is presented in the form of confusion matrices, giving the number of correct and false classifications, from which probabilities of correct classification have been calculated for the four objects.

Separate studies have been made of the clutter-free case, and with grass background.

In the clutter-free case, the study shows (Figure 4.6 and 4.7) that only the fully polarimetric system attains good performance levels, with a probability of correct classification of the order of 90%. Moreover, this system must operate in combination with dense angular spacing of catalogue target data and high range resolution. The angle increment in the stored data must be less than about 0.1° , which somewhat exceeds the angular fluctuation ("glint") period of target returns, which is about 0.01° at 94 GHz. The dependence on range resolution is strong, and the requirement for the above performance is that the range resolution should be a fraction of the mean distance between the reflectors in the models, or less than about 0.3 m. This is in agreement with the findings of the M.I.T. Lincoln Laboratory for its 35 GHz airborne SAR that it is very difficult to perform classification with 1×1 m ground resolution for the type of targets in question. This lends some credence to the applicability of the approach used in the present report.

The single channel system has a performance which generally lies some tens of percent below that of the fully polarimetric one, in terms of probability of correct classification.

The introduction of clutter produces severe deterioration of the performance. This result is crucially dependent on correct relative strengths of the target and clutter returns, and must be investigated closer; there is a strong need for polarimetric, high-resolution measurements of real targets and background to provide the necessary information. However, the reduction of the influence of clutter may be expected to remain a major challenge. Doppler techniques and Synthetic Aperture schemes are two methods to alleviate the problems.

Successful recognition hinges on the combination of polarimetric analysis and high spatial resolution, which isolates single reflectors in resolution cells of the radar. The basic required ability of a real-world radar to recognize such single reflectors has been demonstrated experimentally in this work. This was made with a coherent, fully polarimetric 94 GHz radar, which measured the returns from 23 single reflectors of two basic kinds, made up of orthogonal surfaces forming a corner or dihedral, respectively. These could be classified with 100% accuracy, from a choice within a created canonical set of 8 different reflector types. Furthermore, the roll orientation of the dihedral-type reflectors could be determined with an accuracy close to that of a mechanical measurement with a spirit level.

The use of the produced models is not restricted to classification studies, but they may also be seen as generators of target and background data for coherent, polarimetric sensors in other applications under study. Such data can be obtained with relatively short computer runs with these models. However, a draw-back of modelling the clutter on the same principle as the targets is a decrease of physical correspondence between the model and the real-world scattering.

Appendix Polarisation concepts

A.1 The scattering matrix

The general polarisation state of a radar wave of a specific frequency ω is elliptical, which means that the end-point of the electric field vector drawn from a fixed observation point P (Figure A.1) traces an ellipse in space as a function of time.

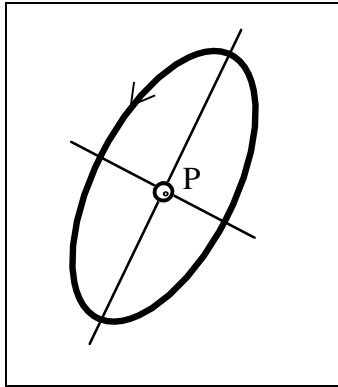


Figure A.1 The polarisation ellipse in a plane perpendicular to the direction of propagation (out from the paper). The figure illustrates "right" hand rotation of the tip of the electric field vector, according to the IEEE definition, i.e. in agreement with the direction of tightening a right-handed screw, seen in the direction of propagation. The ellipse is characterised by its size, shape, orientation and direction of rotation of the field vector.

If the radar wave is scattered by a target its polarisation state is generally changed, see Figure A.2.

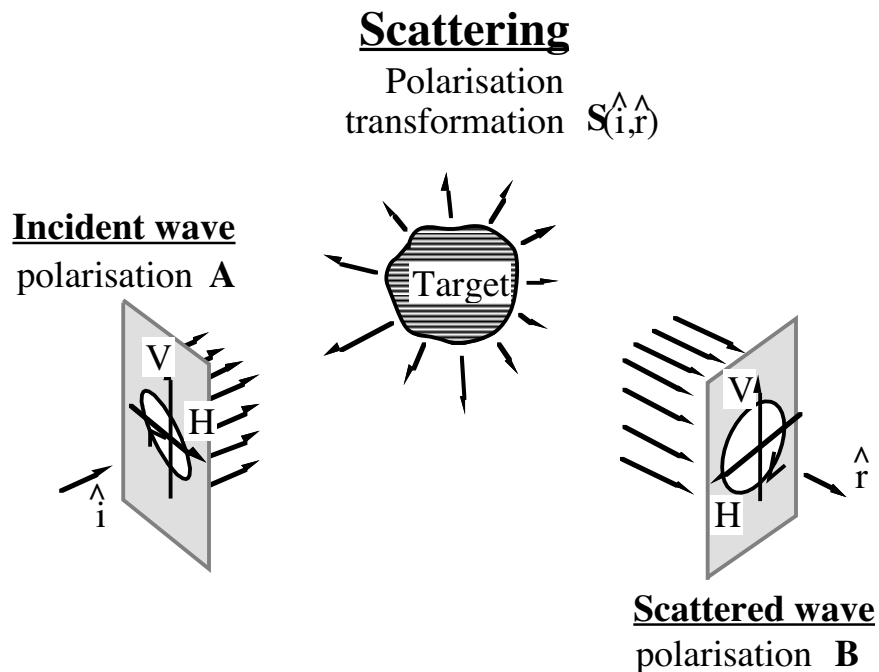


Figure A.2 Schematic illustration of the transformation by a scattering object of the elliptical polarisation of an incident wave into another elliptical polarisation of the scattered wave.

The transformation between the incident and the scattered waves is in almost all practical cases linear, and can be expressed as

$$E'_1 = s_{11}E_1 + s_{12}E_2, \quad (\text{A.1a})$$

$$E'_2 = s_{21}E_1 + s_{22}E_2. \quad (\text{A.1b})$$

Here E'_1, E'_2 and E_1, E_2 are the (complex) vector components of the scattered and the incident wave, respectively, in a coordinate system which is perpendicular to the propagation. The field is transversal (in vacuum), and can hence be described by two orthogonal components. The four complex numbers $s_{11}, s_{12}, s_{22}, s_{21}$ describe the scattering. [The radar cross section σ is proportional to the square of the corresponding magnitudes, *e.g.* $\sigma_{11} \propto |s_{11}|^2$]. In the monostatic case $s_{12} = s_{21}$. Often, linear polarisation is used with components given in a horizontal/vertical system, but (A.1) is equally valid if the components refer to right and left circular polarisation, for example.

In matrix form we have

$$\mathbf{E}' = \mathbf{S}\mathbf{E}. \quad (\text{A.2})$$

Here,

$$\mathbf{E}' = \begin{pmatrix} E'_1 \\ E'_2 \end{pmatrix}, \text{ and } \mathbf{E} = \begin{pmatrix} E_1 \\ E_2 \end{pmatrix}, \quad (\text{A.3})$$

and the **polarisation matrix** (or the **scattering matrix**) is given by

$$\mathbf{S} = \begin{pmatrix} s_{11} & s_{12} \\ s_{21} & s_{22} \end{pmatrix}. \quad (\text{A.4})$$

The polarisation matrix is the basis for polarimetric description of target scattering. It contains information about both the change in phase and in amplitude through the scattering in the target, and is in that sense a complete description; it is coherent, and is a characterization in terms of field strength.

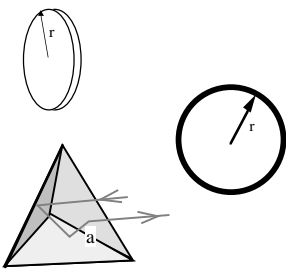
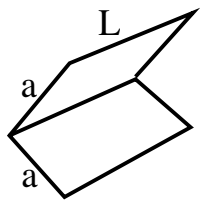
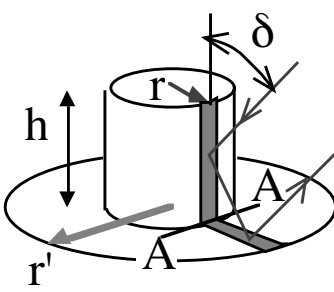
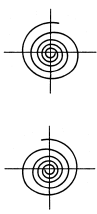
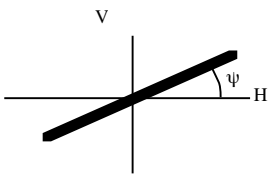
A common phase factor can be extracted from the matrix and can usually be excluded from the polarisation description. Hence, in the monostatic case with a symmetric matrix the polarimetric scattering is described by 5 real parameters.

Table A.1 shows some simple reflector types and their polarisation matrices, in the short wavelength approximation. Reflectors of this kind, where the radar echo is produced by multiple reflections, can be assigned to the two types "odd" and "even", depending on if

the number of reflections is odd or even. The scattering matrix with circular basis, $\begin{pmatrix} s_{RR} & s_{RL} \\ s_{LR} & s_{LL} \end{pmatrix}$

(R="Right", L="Left") for the two types is characterized by the fact that the return power in the "odd" case is obtained in the two orthogonally polarised channels ($s_{RL}, s_{LR} \neq 0$) with none in the two other ones ($s_{RR}, s_{LL} = 0$). For an "even" reflector all return power occurs in the two like-polarised channels, *i.e.* $s_{RR}, s_{LL} \neq 0$, whereas $s_{RL}, s_{LR} = 0$.

Table A.1 Some simple reflector types, their far field polarisation matrices and maximum radar cross sections, in short-wavelength approximation.

| | Reflector | Normalised polarisation matrix Linear basis (H,V) Circular basis (R,L) | Maximum radar cross section |
|---|---|--|--|
|  | Flat plate Sphere Trihedral with triangular sides | $\mathbf{S}_{lin} = \begin{pmatrix} -1 & 0 \\ 0 & -1 \end{pmatrix}$ $\mathbf{S}_{circ} = \begin{pmatrix} 0 & -1 \\ -1 & 0 \end{pmatrix}$ | $\frac{4\pi^3 r^4}{\lambda^2}$ πr^2 $\frac{4\pi a^4}{3\lambda^2}$ |
|  | Right-angle dihedral ; the tilt angle of the seam with respect to the horizontal = ψ | $\mathbf{S}_{lin} = \begin{pmatrix} \cos 2\psi & \sin 2\psi \\ \sin 2\psi & -\cos 2\psi \end{pmatrix}$ $\mathbf{S}_{circ} = \begin{pmatrix} e^{-i2\psi} & 0 \\ 0 & e^{i2\psi} \end{pmatrix}$ | $\frac{8\pi a^2 L^2}{\lambda^2}$ |
|  | Cylinder hat A narrow band (shaded) contributes to the radar return which is of dihedral type. The seam A-A forms an angle ψ with the horizontal | $\mathbf{S}_{lin} = \begin{pmatrix} \cos 2\psi & \sin 2\psi \\ \sin 2\psi & -\cos 2\psi \end{pmatrix}$ $\mathbf{S}_{circ} = \begin{pmatrix} e^{-i2\psi} & 0 \\ 0 & e^{i2\psi} \end{pmatrix}$ | $\min \left[\frac{8\pi r h^2 \sin \delta}{\lambda}, \frac{\lambda}{8\pi r (r' - r)^2 \cos^2 \delta}, \frac{1}{\lambda \sin \delta} \right]$ |
|  | Right hand helix Left hand helix | $\mathbf{S}_{lin} = \frac{1}{2} \begin{pmatrix} 1 & -i \\ -i & -1 \end{pmatrix}$ $\mathbf{S}_{circ} = \begin{pmatrix} 0 & 0 \\ 0 & 1 \end{pmatrix}$ $\mathbf{S}_{lin} = \frac{1}{2} \begin{pmatrix} 1 & i \\ i & -1 \end{pmatrix}$ $\mathbf{S}_{circ} = \begin{pmatrix} 1 & 0 \\ 0 & 0 \end{pmatrix}$ | σ_{helix} |
|  | Line , tilt angle with respect to the horizontal = ψ | $\mathbf{S}_{lin} = \begin{pmatrix} -\cos^2 \psi & -\sin \psi \cos \psi \\ -\sin \psi \cos \psi & -\sin^2 \psi \end{pmatrix}$ $\mathbf{S}_{circ} = \frac{1}{2} \begin{pmatrix} -e^{-i2\psi} & -1 \\ -1 & -e^{i2\psi} \end{pmatrix}$ | σ_{line} |

A.2 Target decomposition

A general, complex 2×2 matrix, \mathbf{A} , can be expanded in a set of base matrices. One common choice of base is the so-called Pauli set (Arfken and Weber, 1995, p. 196). These can be defined in slightly different ways; Cloude (1986) uses

$$\sigma_0 = \begin{pmatrix} 1 & 0 \\ 0 & 1 \end{pmatrix}, \sigma_1 = \begin{pmatrix} 1 & 0 \\ 0 & -1 \end{pmatrix}, \sigma_2 = \begin{pmatrix} 0 & 1 \\ 1 & 0 \end{pmatrix}, \sigma_3 = \begin{pmatrix} 0 & -i \\ i & 0 \end{pmatrix}. \quad (\text{A.5})$$

The expansion of \mathbf{A} can then be written

$$\begin{aligned} \mathbf{A} &= \begin{pmatrix} a_{11} & a_{12} \\ a_{21} & a_{22} \end{pmatrix} = a_0 \sigma_0 + a_1 \sigma_1 + a_2 \sigma_2 + a_3 \sigma_3 \\ &= a_0 \begin{pmatrix} 1 & 0 \\ 0 & 1 \end{pmatrix} + a_1 \begin{pmatrix} 1 & 0 \\ 0 & -1 \end{pmatrix} + a_2 \begin{pmatrix} 0 & 1 \\ 1 & 0 \end{pmatrix} + a_3 \begin{pmatrix} 0 & -i \\ i & 0 \end{pmatrix}. \end{aligned} \quad (\text{A.6})$$

If \mathbf{A} is a scattering matrix representing a monostatic case (symmetric matrix), the last term in (A.6) must be zero ($a_3 = 0$). The remaining three terms in the rightmost membrum of (A.6) can be visualised as representing the coherent backscatter from a trihedral, a dihedral with $\psi = 0^\circ$ and a dihedral with $\psi = 45^\circ$, cf. Table A.1 and Figure A.3.

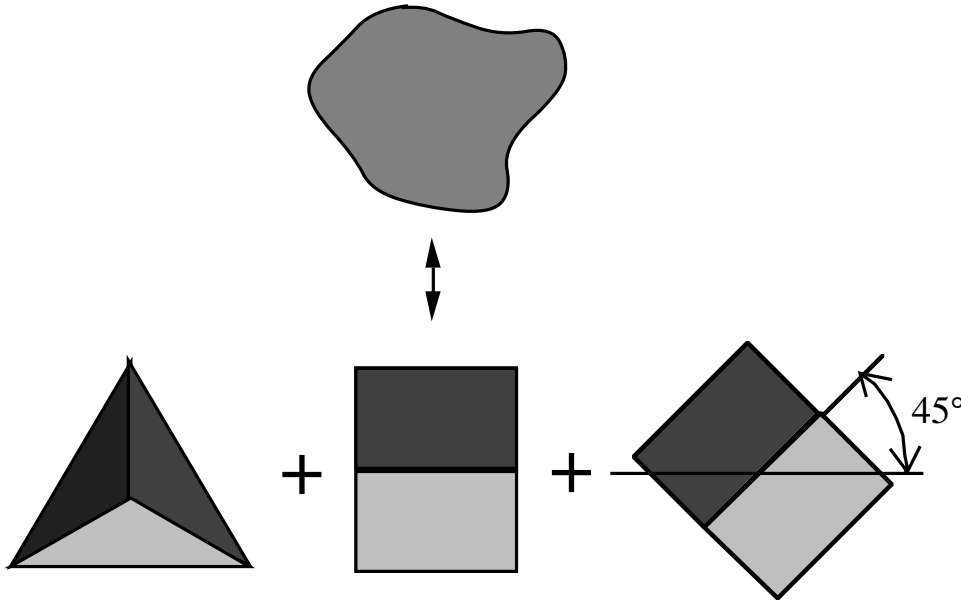


Figure A.3 At short wavelengths, the backscattering from a general target (top) can be seen as the sum of backscatter from a trihedral and two dihedrals with different tilt angles.

A.3 Stokes' polarisation description, the Mueller matrix and the Huynen parameters

A.3.1 Stokes' parameters and the Mueller matrix

Sometimes, using power quantities may have be of some advantage when describing polarisation concepts. This is especially so with stochastically varying fields (Huynen, 1987). A commonly used description is based on Stokes' parameters for a radar wave, which are defined as follows.

| | |
|---------|---|
| g_0 : | total power of the wave |
| g_1 : | difference between left-hand and right-hand circularly polarised power |
| g_2 : | difference between horizontally and vertically polarised power |
| g_3 : | difference between linearly polarised power along directions at $+45^\circ$ and -45° to the horizontal |

These parameters can be collected into a four-dimensional vector, **Stokes' vector**

$$\mathbf{g} = \begin{pmatrix} g_0 \\ g_1 \\ g_2 \\ g_3 \end{pmatrix}. \quad (\text{A.7})$$

When the wave is scattered in a target the vector transforms into \mathbf{g}' . The transformation is linear in practically all cases and can be expressed by a real 4×4 -matrix, the **Stokes'** or **Mueller**-matrix \mathbf{M} as

$$\mathbf{g}' = \mathbf{M}\mathbf{g} = \begin{pmatrix} m_{00} & m_{01} & m_{02} & m_{03} \\ m_{10} & m_{11} & m_{12} & m_{13} \\ m_{20} & m_{21} & m_{22} & m_{23} \\ m_{30} & m_{31} & m_{32} & m_{33} \end{pmatrix} \begin{pmatrix} g_0 \\ g_1 \\ g_2 \\ g_3 \end{pmatrix} \quad (\text{A.8})$$

The Mueller matrix elements can be expressed with the scattering matrix coefficients $s_{HH}, s_{HV}, s_{VH}, s_{VV}$ via quadratic expressions as follows (Lin, 1990; Sume, 1992):

$$\begin{aligned} m_{00} &= \frac{1}{4}(s_{HH}s_{HH}^* + s_{VV}s_{VV}^* + 2s_{HV}s_{HV}^*), \\ m_{11} &= \frac{1}{4}(2s_{HV}s_{HV}^* - s_{HH}s_{VV}^* - s_{HH}^*s_{VV}), \\ m_{22} &= \frac{1}{4}(s_{HH}s_{HH}^* + s_{VV}s_{VV}^* - 2s_{HV}s_{HV}^*), \\ m_{33} &= \frac{1}{4}(s_{HH}s_{VV}^* + s_{HH}^*s_{VV} + 2s_{HV}s_{HV}^*), \\ m_{01} &= -\frac{i}{4}(s_{HH}s_{HV}^* - s_{HH}^*s_{HV} + s_{VV}s_{HV}^* - s_{VV}^*s_{HV}), \end{aligned}$$

$$\begin{aligned}
m_{02} &= \frac{1}{4}(s_{HH}s_{HH}^* - s_{VV}s_{VV}^*), \\
m_{03} &= \frac{1}{4}(s_{HH}s_{HV}^* + s_{HH}s_{HV}^* + s_{VV}s_{HV}^* + s_{VV}s_{HV}^*), \\
m_{12} &= -\frac{i}{4}(s_{HH}s_{HV}^* - s_{HH}s_{HV}^* - s_{VV}s_{HV}^* + s_{VV}s_{HV}^*), \\
m_{13} &= -\frac{i}{4}(s_{HH}s_{VV}^* - s_{HH}s_{VV}^*), \\
m_{23} &= \frac{1}{4}(s_{HH}s_{HV}^* + s_{HH}s_{HV}^* - s_{VV}s_{HV}^* - s_{VV}s_{HV}^*), \\
m_{10} &= m_{01}, m_{20} = m_{02}, m_{30} = m_{03}, m_{21} = m_{12}, m_{31} = m_{13}, m_{32} = m_{23}.
\end{aligned} \tag{A.9}$$

A.3.2 Huynen's parameters

The Huynen parameters [Huynen (1987)], are defined by writing

$$\mathbf{g}' = \mathbf{M}\mathbf{g} = \begin{pmatrix} A_0 + B_0 & F & C_\psi & H_\psi \\ F & -A_0 + B_0 & G_\psi & D_\psi \\ C_\psi & G_\psi & A_0 + B_\psi & -E_\psi \\ H_\psi & D_\psi & -E_\psi & A_0 - B_\psi \end{pmatrix} \begin{pmatrix} g_0 \\ g_1 \\ g_2 \\ g_3 \end{pmatrix}, \tag{A.10}$$

The parameters indexed with ψ mark that they depend on the target orientation relative to the horizontal direction. More specifically, the angle ψ is the tilt angle of the polarisation ellipse of the (generally elliptic) polarisation that gives the maximum radar return from the target, for a fixed aspect angle, see Figure A.4.

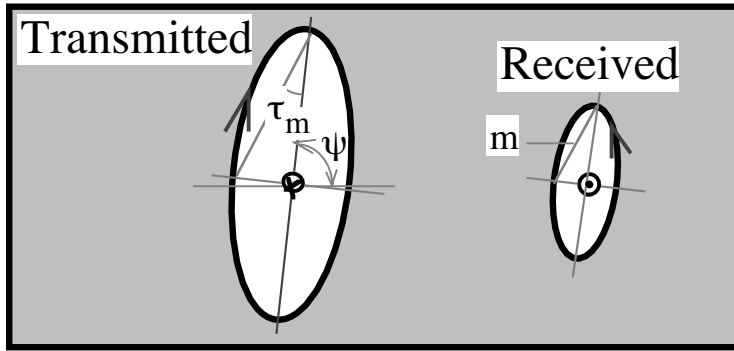


Figure A.4 Every radar target has, for a fixed aspect angle, a *maximum polarisation*, characterized by:
(a) It gives the maximum radar return for the aspect angle.
(b) It is polarimetrically matched to the target: the scattering in the target does not change the form, orientation or sense of rotation (seen along the direction of propagation) of the polarisation ellipse.

If the target is rotated about the line of sight to the radar so that ψ becomes zero ("de- ψ -ing" in Huynen's terminology), the parameters will generally take on new values, which are denoted by omission of their indexes, *i.e.* $B_\psi(\psi = 0) \equiv B$ etc. It can be shown (Huynen, 1987) that the angle dependence of the Huynen parameters is given explicitly in terms of these "de- ψ -ed" parameters by

$$H_{\psi} = C \sin 2\psi , \quad (\text{A.11.a})$$

$$C_{\psi} = C \cos 2\psi , \quad (\text{A.11.b})$$

$$G_{\psi} = G \cos 2\psi - D \sin 2\psi , \quad (\text{A.11.c})$$

$$D_{\psi} = G \sin 2\psi + D \cos 2\psi , \quad (\text{A.11.d})$$

$$E_{\psi} = E \cos 4\psi - B \sin 4\psi , \quad (\text{A.11.e})$$

$$B_{\psi} = E \sin 4\psi + B \cos 4\psi . \quad (\text{A.11.f})$$

We note that $H = 0$ according to (A.11.a).

The "de- ψ -ed" parameters are associated with geometrical properties of the target according to Table A2, and have been used in the present work for classification, see Section 4.4.1.

Table A.2 *Geometrical significance of the Huynen parameters.*

| | |
|--------------------|--|
| A_0 | is related to target symmetry: can be seen as return power from regular, even, convex parts of the scatterer; for a sphere this is the only non-zero parameter |
| B_0 | is related to target structure: can be seen as return power from the irregular, uneven, non-convex parts |
| B_0-B | is related to non-symmetry |
| B_0+B | is related to target irregularity |
| C and D | are related to target shape |
| E and F | are related to target twist |
| G and H | are related to coupling between different parts of the target |
| More specifically: | |
| C | defines global shape (a line target has large C) |
| D | defines local shape (curvature difference; discontinuities e.g. an edge) |
| E | defines local twist or surface torsion |
| F | defines global twist or target helicity |
| G | defines local coupling |
| H_{ψ} | defines global coupling due to target orientation (roll angle ψ) |

Since a non-varying target can be described with five independent parameters, as mentioned in Section A.1, the nine Huynen parameters are not indepent. There are four relations between them in this case.

The polarisation description using the Stokes/Mueller/Huynen formalism is an example of a phenomenological approach, characterized by being essentially non-committal concerning the detailed scattering mechanism. Its aim is to draw general conclusions about every radar target, using the tools of linear algebra. The resulting scheme of description is, among other things, wavelength independent, whereas the coefficients that appear in it are not. It is to be expected that such a formalism is somewhat blunt, since it is generally not tailored for the application at hand. A manifestation of this can be seen from Table A2: the interpretation of the Huynen parameters reflects quite general properties of the targets. In specific applications, model-based methods can be expected to be more effective for classification. However, for an initial investigation like the present one, the generality of the phenomenological approach may be of decisive advantage.

A.4 The Huynen parameters from the scattering matrix

A.4.1 The computational problem

The calculation of the "de- ψ -ed" Huynen parameters $A_0, B_0 + B, B_0 - B, C, D, E, F, G$ from the scattering matrix elements proceeds by in itself simple algebra. However, special attention has to be paid to the simple reflector types which occur in the modelling, where the general algorithm fails. It is felt valuable to have documented here the calculation scheme used in the present work.

From the expressions (A.9) and (A.10) it is easy to calculate the parameters $A_0, B_0, B_\psi, C_\psi, D_\psi, E_\psi, F_\psi, G_\psi, H_\psi$ from the scattering matrix elements. For the determination of the "de- ψ -ed" variants from (A.11), the angle ψ is required. The calculation of ψ is the step that requires special attention to specific simple reflector cases. In the general case ψ is calculated as described by Kjellgren *et al.* (1992) and Sume (1992), and will not be further discussed here. Instead, we will focus on the specific cases.

It is of computational and conceptual advantage to rewrite the scattering matrix in the following way, introducing three (complex) parameters a, b, c , the coefficients in the Pauli expansion (A.6) of a symmetric matrix, which contain the same information as the elements $s_{HH}, s_{HV}, s_{VH}, s_{VV}$ and which can be visualized as depicted by Figure A.3:

$$\mathbf{S} = \begin{pmatrix} a + b & c \\ c & a - b \end{pmatrix}, \quad (\text{A.12})$$

where

$$a = \frac{s_{HH} + s_{VV}}{2}, \quad (\text{A.13.a})$$

$$b = \frac{s_{HH} - s_{VV}}{2}, \quad (\text{A.13.b})$$

$$c = s_{HV} = s_{VH}. \quad (\text{A.13.c})$$

The special cases occur for $|a| = 0, |b| = 0$ and/or $|c| = 0$, which gives the structure shown in Figure A.5 for the calculation of ψ [after Krogager (1993), with some modifications, see footnote 9].

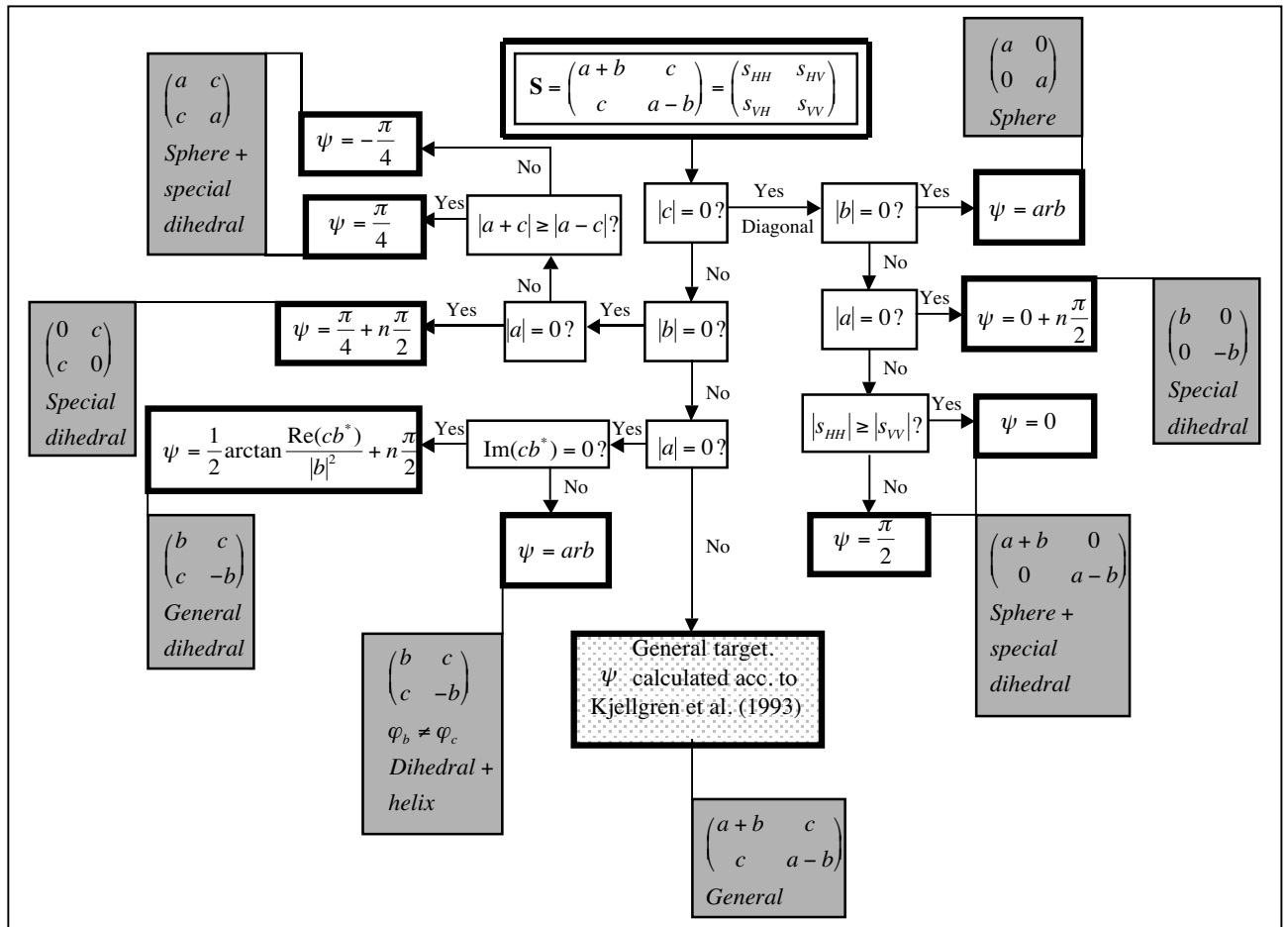


Figure A.5 Scheme for calculation of the tilt angle ψ of the maximum polarisation ellipse of a target with scattering matrix \mathbf{S} [after Krogager (1993), with some modifications]. The procedure for a general target follows down the vertical path, and ψ is calculated as described by Kjellgren *et al.* (1993). Special cases are found as ramifications to the left or right from this main branch. The label "special dihedral" denotes a dihedral with a specific tilt angle ($0, \pm\pi/4, \pm\pi/2$), which gives the proper scattering matrix contribution.

A.4.2 The tilt angle ψ from diagonalization of the scattering matrix (Bickel, 1965)

To comment on Figure A.5 we review Bickel's (1965) study of how a scattering matrix transforms under change of polarisation basis, and specifically the case where the final form is diagonal. This form occurs when the two orthogonal eigenvectors of the scattering matrix are taken as basis vectors in describing the scattering. In fact, the maximum polarisation \mathbf{m} (see Figure A.4) is one eigenvector, and the tilt angle of its polarisation ellipse is the angle ψ . Finding this angle is thus tantamount to solving the eigenvalue problem⁸ for the scattering matrix.

If we denote the other (orthogonal) eigenpolarisation by \mathbf{m}_\perp we have (Huynen, 1987) that \mathbf{S} is brought to diagonal form \mathbf{S}_d by applying the unitary transformation

$$\mathbf{U} = (\mathbf{m}, \mathbf{m}_\perp), \quad (\text{A.14})$$

as

⁸ In recent references called a con-eigenvalue problem, due to a conjugate form in the equation (Horn and Johnson, 1985; Lüneburg, 1995).

$$\mathbf{S}_d = \mathbf{U}^T \mathbf{S} \mathbf{U}, \quad (\text{A.15})$$

where T denotes transpose.

The two eigenpolarisations can be expressed with the tilt angle ψ and the ellipticity angle τ_m of the maximum polarisation [see Figure A.4 and Huynen (1987)]:

$$\mathbf{m} = \mathbf{m}(\psi, \tau_m) = \begin{pmatrix} \cos \psi \cos \tau_m - i \sin \psi \sin \tau_m \\ \sin \psi \cos \tau_m + i \cos \psi \sin \tau_m \end{pmatrix}, \quad (\text{A.16.a})$$

and the orthogonal

$$\mathbf{m}_\perp = \mathbf{m}(\psi + \pi/2, -\tau_m) = \begin{pmatrix} -\sin \psi \cos \tau_m + i \cos \psi \sin \tau_m \\ \cos \psi \cos \tau_m + i \sin \psi \sin \tau_m \end{pmatrix}. \quad (\text{A.16.b})$$

After simple calculations one gets from (A.14) and (A.16)

$$\mathbf{U} = \begin{pmatrix} \cos \psi & -\sin \psi \\ \sin \psi & \cos \psi \end{pmatrix} \begin{pmatrix} \cos \tau_m & i \sin \tau_m \\ i \sin \tau_m & \cos \tau_m \end{pmatrix} \equiv \mathbf{R} \mathbf{E}, \quad (\text{A.17})$$

where

$$\mathbf{R} = \begin{pmatrix} \cos \psi & -\sin \psi \\ \sin \psi & \cos \psi \end{pmatrix} \quad (\text{A.18})$$

represents a rotation by the angle ψ about the line of sight, and

$$\mathbf{E} = \begin{pmatrix} \cos \tau_m & i \sin \tau_m \\ i \sin \tau_m & \cos \tau_m \end{pmatrix} \quad (\text{A.19})$$

represents a change in ellipticity. This means that the transformation of \mathbf{S} from the H, V -representation to the eigenpolarisation $\mathbf{m}, \mathbf{m}_\perp$ -representation can be regarded as consisting of an ellipticity change of the basis vectors, followed by a rotation about the line of sight (Bickel, 1965). The transformation (A.15) can thus be written

$$\mathbf{S}_d = \mathbf{E}^T \mathbf{R}^T \mathbf{S} \mathbf{R} \mathbf{E} = \mathbf{E}^T \mathbf{S}' \mathbf{E}, \quad (\text{A.20})$$

where the matrix resulting from the rotation is

$$\mathbf{S}' = \mathbf{R}^T \mathbf{S} \mathbf{R}, \quad (\text{A.21})$$

and the ellipticity change produces

$$\mathbf{S}_d = \mathbf{E}^T \mathbf{S}' \mathbf{E}. \quad (\text{A.22})$$

It is convenient to define

$$s_1 = s_{HH} + s_{VV}, \quad (\text{A.23.a})$$

$$s_2 = s_{HH} - s_{VV}, \quad (\text{A.23.b})$$

$$s_{12} = s_{HV}. \quad (\text{A.23.c})$$

From (A.18) and (A.21) one gets for the elements of \mathbf{S}' ⁹

$$s'_1 = s_1, \quad (\text{A.24.a})$$

$$s'_2 = s_2 \cos 2\psi + 2s_{HV} \sin 2\psi, \quad (\text{A.24.b})$$

$$2s'_{12} = 2s_{12} \cos 2\psi - s_2 \sin 2\psi. \quad (\text{A.24.c})$$

One obtains from (A.19) and (A.20)

$$s_{d1} = s_1 \cos 2\tau_m + i2s'_{12} \sin 2\tau_m, \quad (\text{A.25a})$$

$$s_{d2} = s'_2, \quad (\text{A.25b})$$

$$2s_{d12} = 2s'_{12} \cos 2\tau_m + is_1 \sin 2\tau_m. \quad (\text{A.25c})$$

The combination of (A.23)-(A.25) gives the final expressions for the elements of the diagonalized scattering matrix

$$s_{d11} = a \cos 2\tau_m + b(\cos 2\psi - i \sin 2\psi \sin 2\tau_m) + c(\sin 2\psi + i \cos 2\psi \sin 2\tau_m), \quad (\text{A.26a})$$

$$s_{d22} = a \cos 2\tau_m - b(\cos 2\psi + i \sin 2\psi \sin 2\tau_m) - c(\sin 2\psi - i \cos 2\psi \sin 2\tau_m), \quad (\text{A.26b})$$

$$s_{d12} = ai \sin 2\tau_m - b \sin 2\psi \cos 2\tau_m + c \cos 2\psi \cos 2\tau_m. \quad (\text{A.26c})$$

The condition of diagonal form is $s_{d12} = s_{d21} = 0$, which applied to (A.25c) gives

$$\tan 2\tau_m = \frac{i2s'_{12}}{s_1}. \quad (\text{A.27})$$

This only has meaning for real values of τ_m when the orientation of the polarisation ellipse of the maximum polarisation is such that

$$\text{Re } s'_{12}s_1^* = 0, \quad (\text{A.28})$$

so that from (A.24c) ψ is given by¹⁰

$$\tan 2\psi = \frac{+2 \text{Re } s_1^* s_{12}}{\text{Re } s_1^* s_2}. \quad (\text{A.29})$$

Introducing the parameters a, b, c with $s_1 = 2a$, $s_2 = 2b$, $s_{12} = c$, we get

$$\psi = \frac{1}{2} \arctan \frac{\text{Re}(a^* c)}{\text{Re}(a^* b)}, \quad (\text{A.30})$$

⁹ The two explicitly written signs in (A.24b) and (A.24c) are reversed compared to Bickel (1965), whose result is reproduced in Krogager (1993). The signs in (A.24) have been obtained both by hand calculation and by *Mathematica*. Furthermore, the final result (A.26) agrees with Wei *et al.* (1986).

¹⁰ The sign is different from Bickel (1965) due to the discrepancy noted for (A.24).

which is the final result for a general scattering matrix. As mentioned above the calculation of ψ for the general case is made using a different method for solving the eigenvalue equation for the scattering matrix, developed and used in previous FOA work (Kjellgren *et al.* 1993). The Bickel scheme will be used for discussing some special cases in the next section.

A.4.3 Special cases

A few cases in the left part of Figure A.5 deserve special comment.

A.4.3.1 General dihedral

The scattering matrix of a general dihedral has the form (Table A.1)

$$\sqrt{\sigma} e^{i\beta} \begin{pmatrix} \cos 2\psi & \sin 2\psi \\ \sin 2\psi & -\cos 2\psi \end{pmatrix} \equiv \begin{pmatrix} b & c \\ c & -b \end{pmatrix} \quad (\text{A.31})$$

Hence

$$\frac{cb^*}{|b|^2} = \frac{\sin 2\psi}{\cos 2\psi}, \quad (\text{A.32})$$

and we can write

$$\tan 2\psi = \frac{\text{Re } cb^*}{|b|^2}. \quad (\text{A.33})$$

Thus

$$\psi = \frac{1}{2} \arctan \frac{\text{Re } cb^*}{|b|^2} + n \frac{\pi}{2}. \quad (\text{A.34})$$

A.4.3.2 Dihedral+helix

This case has a more general scattering matrix than the previous one and is characterized by unequal phases for b and c , *i.e.* $\varphi_b \neq \varphi_c$ in the scattering matrix

$$\begin{pmatrix} b & c \\ c & -b \end{pmatrix}. \quad (\text{A.35})$$

This is Huynen's (1987, p. 69-70) N-Target, which can be modelled as a dihedral and a helix, *cf* Table A.1. The maximum polarisation of the helix is circular, *i.e.* its $|\tau_m| = \pi/4$, whereas the ellipticity angle for the maximum polarisation is arbitrary for the dihedral. Hence, the combined configuration has a maximum polarisation that is circular, from which follows that ψ is arbitrary.

A.4.3.3 Sphere+special dihedral

We consider the case $|b| = 0, |a| \neq 0$, *i.e.* the scattering matrix

$$\mathbf{S} = \begin{pmatrix} a & c \\ c & a \end{pmatrix}. \quad (\text{A.36})$$

This can be written

$$\mathbf{S} = e^{i\pi} |a| e^{i\varphi_a} \begin{pmatrix} -1 & 0 \\ 0 & -1 \end{pmatrix} + |c| e^{i\varphi_c} \begin{pmatrix} 0 & 1 \\ 1 & 0 \end{pmatrix}, \quad (\text{A.37})$$

where φ_a, φ_c are the phases of a and c , respectively. From this expression of \mathbf{S} we see that it can be interpreted as a sphere plus a special dihedral. The ellipticity angle τ_m of the maximum polarisation for these reflectors are 0 and arbitrary, respectively. This angle for the configuration sphere+dihedral is hence $\tau_m = 0$; this also follows from the fact that it is a symmetric target (Huynen, 1987), *i.e.* has an axis of symmetry perpendicular to the line of sight. Introducing $|b| = 0, \tau_m = 0$ in (A.26), we have for the diagonal form of the scattering matrix

$$s_{d11} = a + c \sin 2\psi, \quad (\text{A.38a})$$

$$s_{d22} = a - c \sin 2\psi, \quad (\text{A.38b})$$

$$0 = c \cos 2\psi. \quad (\text{A.38c})$$

Hence, $\psi = \pm\pi/4$. The diagonal elements s_{d11}, s_{d22} are the two eigenvalues, where in Huynen's (1987) convention $|s_{d11}| \geq |s_{d22}|$. If we insert $\psi = \pi/4$ in (A.38) we have

$$s_{d11} = a + c, \quad (\text{A.39a})$$

$$s_{d22} = a - c. \quad (\text{A.39b})$$

Hence, if $|a + c| \geq |a - c|$ then $\psi = \pi/4$ is the correct choice, else $\psi = -\pi/4$. Similarly, with $\psi = -\pi/4$ introduced in (A.38) we have

$$s_{d11} = a - c, \quad (\text{A.40a})$$

$$s_{d22} = a + c. \quad (\text{A.40b})$$

Hence, if $|a - c| \geq |a + c|$ then $\psi = -\pi/4$, else $\psi = \pi/4$, and the scheme in Figure A.5 follows.

References

Arfken, George B., Weber, Hans J.: *Mathematical Methods for Physicists*. 4th ed., San Diego: Academic Press, 1029pp, 1995. ISBN 0-12-059815-9.

Bar-Yam, Yaneer: *Dynamics of Complex Systems*. Reading: Addison-Wesley, 1997, ISBN 0-201-55748-7.

Bickel, S.H.: "Some Invariant Properties of the Polarization Scattering Matrix", *Proceedings of the IEEE*, vol. 53, no. 8, p. 1070-1072, Aug. 1965.

Brock, Billy C.: *Polarimetric Calibration of a Coherent Measurement Radar*. Albuquerque: Sandia National Laboratories, Report SAND91-2150, UC-706, december 1991, 59 s.

Cameron, W.L., Leung, L.K.: "Identification of Elemental Polarimetric Scatterer Responses in High-resolution ISAR and SAR Signature Measurements", *Proceedings of the Second International Workshop on Radar Polarimetry, JIPR 92*, Nantes, 8-10 Sept. 1992, p. 196-212. Nantes: IRESTE, 1992. ISBN 2-909805-01-8.

Cloude, S.R.: *Polarimetry: The Characterisation of Polarisation Effects in EM Scattering*. Ph.D. Thesis, University of Birmingham, 1986.

Currie, C.H., Currie, N.C.: "MMW Reflectivity Measurement Techniques", Chap. 17 in N.C. Currie and C.E. Brown (ed.), *Principles and Applications of Millimeter-Wave Radar*. Norwood: Artech House, 1987. ISBN 0-89006-202-1.

Currie, N.C., Zehner, S.P.: "Millimeter Wave Land Clutter Model", *IEE Radar 82 Record*, London, September 1982, p. 385-389.

Currie, N.C., Zehner, S.P., Dyer, F.B.: "MMW Land Clutter Model Update". *IEE Radar 87 Digest*, London, October 1987, p. 217-221.

Dudgeon, Dan E., Lacoss, Richard T.: "An Overview of Automatic Target Recognition", *The Lincoln Laboratory Journal*, vol. 6, no. 1, p. 3-10, 1993.

Horn, R.A., Johnson, Ch.A.: *Matrix Analysis*. Cambridge: Cambridge University Press, 1985, ISBN 0 521 30586 1.

Huynen, J.R.: *Phenomenological Theory of Radar Targets*. Ph.D. Thesis, Delft Technical University, Rotterdam, 1970. First Revision. Los Altos Hills, California: P.Q. Research, Nov. 1987.

Johansson, Conny, Sume, Ain: "Polarimetrisk kalibrering av koherent radar med tillämpning vid 94 GHz". Linköping: FOI-R--0161--SE, 77 pp., August 2001 (in Swedish).

Karlsson, Mikael, Lauberts, Andris, Nilsson, Stefan, Nygård, Jonas, Sume, Ain. Linköping: FOA-RH—99-00443, June 1999, (classified).

Kjellgren, Jan, Nilsson, Stefan, Sume, Ain: "A Polarimetric Radar Model for Tank Targets at Millimetre Wavelengths", *Proceedings of the Second International Workshop on Radar Polarimetry, JIPR 92*, Nantes, 8-10 Sept. 1992, p. 138-148. Nantes: IRESTE, 1992. ISBN 2-909805-01-8.

Kjellgren, Jan, Nilsson, Stefan, Sume, Ain: "A Simple Reflector Model for Polarimetric Radar at Millimetre Waves", *International Geoscience and Remote Sensing Symposium (IGARSS' 93)*. Kogaku University, Tokyo, Japan, 18-21 Aug. 1993, p. 2037-2039. Piscataway: IEEE, 1993. ISBN 0-7803-1240-6.

Krogager, E.: *Aspects of Polarimetric Radar Imaging*. Ph.D. Thesis, Technical University of Denmark, Lyngby, 1993.

Lin, S.M.: "On the Huynen's Target Characteristic Parameters", *Antennas and Propagation Symposium Digest*, 7-11 May 1990, Dallas, Texas, p. 562-565. IEEE, 1990.

Lüneburg, E.: "Principles of Radar Polarimetry", *IEICE Trans. Electron.*, vol. E78-C, no. 10, pp. 1339-1345, Oct. 1995.

Nilsson, Stefan: "Datorprogram för studium av radarreturen för en stridsvagn", Linköping: FOA C 30579-8.2,3.2,3.3, 57 pp., July 1990 (in Swedish).

Novak, L.M., Netishen, C.M.: "Polarimetric Synthetic Aperture Radar Imaging", *International Journal of Imaging Systems and Technology*, vol. 4, p. 306-318, 1992.

Novak, L.M., Halversen, S.D., Owirka, G.J., Heitt, M.: "Effects of Polarization and Resolution on the Performance of a SAR Automatic Target Recognition System", *EUSAR'96*, Königswinter, Germany, 1996, p. 89-92.

Sume, A.: "Radarreturen från ett system av diskreta reflektorer". Linköping: FOA A 30064-3.3, 100 pp., August 1992 (in Swedish).

Titin-Schnaider, C.: "Polarimetric analysis of RAMSES SAR images", *Proceedings of the Fourth International Workshop on Radar Polarimetry, JIPR 98*, Nantes, 13-17 July 1998, p. 366-375. Nantes: IRESTE, 1998. ISBN 2-909805-09-3.

Wei, P.S.P., Huynen, J.R., Bradley, T.C.: "Transformation of polarisation bases for radar target scattering matrix", *Electronics Letters*, vol. 22, no. 1, p. 13-14, January 1986.

